International Journal of Physical Sciences

Volume 8 Number 35 23 September, 2013
ISSN 1992-1950

Academic Journals

ABOUT IJPS

The **International Journal of Physical Sciences (IJPS)** is published weekly (one volume per year) by Academic Journals.

International Journal of Physical Sciences (IJPS) is an open access journal that publishes high-quality solicited and unsolicited articles, in English, in all Physics and chemistry including artificial intelligence, neural processing, nuclear and particle physics, geophysics, physics in medicine and biology, plasma physics, semiconductor science and technology, wireless and optical communications, materials science, energy and fuels, environmental science and technology, combinatorial chemistry, natural products, molecular therapeutics, geochemistry, cement and concrete research, metallurgy, crystallography and computer-aided materials design. All articles published in IJPS are peer-reviewed.

Submission of Manuscript

Submit manuscripts as e-mail attachment to the Editorial Office at: ijps@academicjournals.org. A manuscript number will be mailed to the corresponding author shortly after submission.

For all other correspondence that cannot be sent by e-mail, please contact the editorial office (at ijps@academicjournals.org).

The International Journal of Physical Sciences will only accept manuscripts submitted as e-mail attachments.

Please read the **Instructions for Authors** before submitting your manuscript. The manuscript files should be given the last name of the first author.

Editors

Prof. Sanjay Misra
Department of Computer Engineering, School of Information and Communication Technology
Federal University of Technology, Minna,
Nigeria.

Prof. Songjun Li
School of Materials Science and Engineering,
Jiangsu University,
Zhenjiang,
China

Dr. G. Suresh Kumar
Senior Scientist and Head Biophysical Chemistry
Division Indian Institute of Chemical Biology (IICB)(CSIR, Govt. of India),
Kolkata 700 032,
INDIA.

Dr. 'Remi Adewumi Oluyinka
Senior Lecturer,
School of Computer Science
Westville Campus
University of KwaZulu-Natal
Private Bag X54001
Durban 4000
South Africa.

Prof. Hyo Choi
Graduate School
Gangneung-Wonju National University
Gangneung,
Gangwondo 210-702, Korea

Prof. Kui Yu Zhang
Laboratoire de Microscopies et d'Etude de Nanostructures (LMEN)
Département de Physique, Université de Reims,
B.P. 1039. 51687,
Reims cedex,
France.

Prof. R. Vittal
Research Professor,
Department of Chemistry and Molecular Engineering
Korea University, Seoul 136-701,
Korea.

Prof Mohamed Bououdina
Director of the Nanotechnology Centre
University of Bahrain
PO Box 32038,
Kingdom of Bahrain

Prof. Geoffrey Mitchell
School of Mathematics,
Meteorology and Physics
Centre for Advanced Microscopy
University of Reading Whiteknights,
Reading RG6 6AF
United Kingdom.

Prof. Xiao-Li Yang
School of Civil Engineering,
Central South University,
Hunan 410075,
China

Dr. Sushil Kumar
Geophysics Group,
Wadia Institute of Himalayan Geology,
P.B. No. 74 Dehra Dun - 248001(UC)
India.

Prof. Suleyman KORKUT
Duzce University
Faculty of Forestry
Department of Forest Industrial Engineeering
Beciyorukler Campus 81620
Duzce-Turkey

Prof. Nazmul Islam
Department of Basic Sciences & Humanities/Chemistry,
Techno Global-Balurghat, Mangalpur, Near District Jail P.O: Beltalapark, P.S: Balurghat, Dist.: South Dinajpur,
Pin: 733103,India.

Prof. Dr. Ismail Musirin
Centre for Electrical Power Engineering Studies (CEPES), Faculty of Electrical Engineering, Universiti Teknologi Mara,
40450 Shah Alam,
Selangor, Malaysia

Prof. Mohamed A. Amr
Nuclear Physic Department, Atomic Energy Authority
Cairo 13759,
Egypt.

Dr. Armin Shams
Artificial Intelligence Group,
Computer Science Department,
The University of Manchester.

Editorial Board

Prof. Salah M. El-Sayed
Mathematics. Department of Scientific Computing.
Faculty of Computers and Informatics,
Benha University. Benha ,
Egypt.

Dr. Rowdra Ghatak
Associate Professor
Electronics and Communication Engineering Dept.,
National Institute of Technology Durgapur
Durgapur West Bengal

Prof. Fong-Gong Wu
College of Planning and Design, National Cheng Kung University
Taiwan

Dr. Abha Mishra.
Senior Research Specialist & Affiliated Faculty.
Thailand

Dr. Madad Khan
Head
Department of Mathematics
COMSATS University of Science and Technology
Abbottabad, Pakistan

Prof. Yuan-Shyi Peter Chiu
Department of Industrial Engineering & Management
Chaoyang University of Technology
Taichung, Taiwan

Dr. M. R. Pahlavani,
Head, Department of Nuclear physics,
Mazandaran University,
Babolsar-Iran

Dr. Subir Das,
Department of Applied Mathematics,
Institute of Technology, Banaras Hindu University,
Varanasi

Dr. Anna Oleksy
Department of Chemistry
University of Gothenburg
Gothenburg,
Sweden

Prof. Gin-Rong Liu,
Center for Space and Remote Sensing Research
National Central University, Chung-Li,
Taiwan 32001

Prof. Mohammed H. T. Qari
Department of Structural geology and remote sensing
Faculty of Earth Sciences
King Abdulaziz UniversityJeddah,
Saudi Arabia

Dr. Jyhwen Wang,
Department of Engineering Technology and Industrial Distribution
Department of Mechanical Engineering
Texas A&M University
College Station,

Prof. N. V. Sastry
Department of Chemistry
Sardar Patel University
Vallabh Vidyanagar
Gujarat, India

Dr. Edilson Ferneda
Graduate Program on Knowledge Management and IT,
Catholic University of Brasilia,
Brazil

Dr. F. H. Chang
Department of Leisure, Recreation and Tourism Management,
Tzu Hui Institute of Technology, Pingtung 926,
Taiwan (R.O.C.)

Prof. Annapurna P.Patil,
Department of Computer Science and Engineering,
M.S. Ramaiah Institute of Technology, Bangalore-54,
India.

Dr. Ricardo Martinho
Department of Informatics Engineering, School of Technology and Management, Polytechnic Institute of Leiria, Rua General Norton de Matos, Apartado 4133, 2411-901 Leiria,
Portugal.

Dr Driss Miloud
University of mascara / Algeria
Laboratory of Sciences and Technology of Water
Faculty of Sciences and the Technology
Department of Science and Technology
Algeria

Instructions for Author

Electronic submission of manuscripts is strongly encouraged, provided that the text, tables, and figures are included in a single Microsoft Word file (preferably in Arial font).

The **cover letter** should include the corresponding author's full address and telephone/fax numbers and should be in an e-mail message sent to the Editor, with the file, whose name should begin with the first author's surname, as an attachment.

Article Types

Three types of manuscripts may be submitted:

Regular articles: These should describe new and carefully confirmed findings, and experimental procedures should be given in sufficient detail for others to verify the work. The length of a full paper should be the minimum required to describe and interpret the work clearly.

Short Communications: A Short Communication is suitable for recording the results of complete small investigations or giving details of new models or hypotheses, innovative methods, techniques or apparatus. The style of main sections need not conform to that of full-length papers. Short communications are 2 to 4 printed pages (about 6 to 12 manuscript pages) in length.

Reviews: Submissions of reviews and perspectives covering topics of current interest are welcome and encouraged. Reviews should be concise and no longer than 4-6 printed pages (about 12 to 18 manuscript pages). Reviews are also peer-reviewed.

Review Process

All manuscripts are reviewed by an editor and members of the Editorial Board or qualified outside reviewers. Authors cannot nominate reviewers. Only reviewers randomly selected from our database with specialization in the subject area will be contacted to evaluate the manuscripts. The process will be blind review.

Decisions will be made as rapidly as possible, and the journal strives to return reviewers' comments to authors as fast as possible. The editorial board will re-review manuscripts that are accepted pending revision. It is the goal of the IJPS to publish manuscripts within weeks after submission.

Regular articles

All portions of the manuscript must be typed double-spaced and all pages numbered starting from the title page.

The Title should be a brief phrase describing the contents of the paper. The Title Page should include the authors' full names and affiliations, the name of the corresponding author along with phone, fax and E-mail information. Present addresses of authors should appear as a footnote.

The Abstract should be informative and completely self-explanatory, briefly present the topic, state the scope of the experiments, indicate significant data, and point out major findings and conclusions. The Abstract should be 100 to 200 words in length.. Complete sentences, active verbs, and the third person should be used, and the abstract should be written in the past tense. Standard nomenclature should be used and abbreviations should be avoided. No literature should be cited.

Following the abstract, about 3 to 10 key words that will provide indexing references should be listed.

A list of non-standard **Abbreviations** should be added. In general, non-standard abbreviations should be used only when the full term is very long and used often. Each abbreviation should be spelled out and introduced in parentheses the first time it is used in the text. Only recommended SI units should be used. Authors should use the solidus presentation (mg/ml). Standard abbreviations (such as ATP and DNA) need not be defined.

The Introduction should provide a clear statement of the problem, the relevant literature on the subject, and the proposed approach or solution. It should be understandable to colleagues from a broad range of scientific disciplines.

Materials and methods should be complete enough to allow experiments to be reproduced. However, only truly new procedures should be described in detail; previously published procedures should be cited, and important modifications of published procedures should be mentioned briefly. Capitalize trade names and include the manufacturer's name and address. Subheadings should be used. Methods in general use need not be described in detail.

Results should be presented with clarity and precision. The results should be written in the past tense when describing findings in the authors' experiments. Previously published findings should be written in the present tense. Results should be explained, but largely without referring to the literature. Discussion, speculation and detailed interpretation of data should not be included in the Results but should be put into the Discussion section.

The Discussion should interpret the findings in view of the results obtained in this and in past studies on this topic. State the conclusions in a few sentences at the end of the paper. The Results and Discussion sections can include subheadings, and when appropriate, both sections can be combined.

The Acknowledgments of people, grants, funds, etc should be brief.

Tables should be kept to a minimum and be designed to be as simple as possible. Tables are to be typed double-spaced throughout, including headings and footnotes. Each table should be on a separate page, numbered consecutively in Arabic numerals and supplied with a heading and a legend. Tables should be self-explanatory without reference to the text. The details of the methods used in the experiments should preferably be described in the legend instead of in the text. The same data should not be presented in both table and graph form or repeated in the text.

Figure legends should be typed in numerical order on a separate sheet. Graphics should be prepared using applications capable of generating high resolution GIF, TIFF, JPEG or Powerpoint before pasting in the Microsoft Word manuscript file. Tables should be prepared in Microsoft Word. Use Arabic numerals to designate figures and upper case letters for their parts (Figure 1). Begin each legend with a title and include sufficient description so that the figure is understandable without reading the text of the manuscript. Information given in legends should not be repeated in the text.

References: In the text, a reference identified by means of an author‘s name should be followed by the date of the reference in parentheses. When there are more than two authors, only the first author‘s name should be mentioned, followed by ’et al‘. In the event that an author cited has had two or more works published during the same year, the reference, both in the text and in the reference list, should be identified by a lower case letter like ’a‘ and ’b‘ after the date to distinguish the works.

Examples:

Abayomi (2000), Agindotan et al. (2003), (Kelebeni, 1983), (Usman and Smith, 1992), (Chege, 1998; 1987a,b; Tijani, 1993,1995), (Kumasi et al., 2001)

References should be listed at the end of the paper in alphabetical order. Articles in preparation or articles submitted for publication, unpublished observations, personal communications, etc. should not be included in the reference list but should only be mentioned in the article text (e.g., A. Kingori, University of Nairobi, Kenya, personal communication). Journal names are abbreviated according to Chemical Abstracts. Authors are fully responsible for the accuracy of the references.

Examples:

Ogunseitan OA (1998). Protein method for investigating mercuric reductase gene expression in aquatic environments. Appl. Environ. Microbiol. 64:695-702.

Gueye M, Ndoye I, Dianda M, Danso SKA, Dreyfus B (1997). Active N2 fixation in several Faidherbia albida provenances. Ar. Soil Res. Rehabil. 11:63-70.

Charnley AK (1992). Mechanisms of fungal pathogenesis in insects with particular reference to locusts. In: Lomer CJ, Prior C (eds) Biological Controls of Locusts and Grasshoppers: Proceedings of an international workshop held at Cotonou, Benin. Oxford: CAB International, pp 181-190.

Mundree SG, Farrant JM (2000). Some physiological and molecular insights into the mechanisms of desiccation tolerance in the resurrection plant Xerophyta viscasa Baker. In Cherry et al. (eds) Plant tolerance to abiotic stresses in Agriculture: Role of Genetic Engineering, Kluwer Academic Publishers, Netherlands, pp 201-222.

Short Communications

Short Communications are limited to a maximum of two figures and one table. They should present a complete study that is more limited in scope than is found in full-length papers. The items of manuscript preparation listed above apply to Short Communications with the following differences: (1) Abstracts are limited to 100 words; (2) instead of a separate Materials and Methods section, experimental procedures may be incorporated into Figure Legends and Table footnotes; (3) Results and Discussion should be combined into a single section.

Proofs and Reprints: Electronic proofs will be sent (e-mail attachment) to the corresponding author as a PDF file. Page proofs are considered to be the final version of the manuscript. With the exception of typographical or minor clerical errors, no changes will be made in the manuscript at the proof stage.

Copyright: © 2013, Academic Journals.
All rights Reserved. In accessing this journal, you agree that you will access the contents for your own personal use but not for any commercial use. Any use and or copies of this Journal in whole or in part must include the customary bibliographic citation, including author attribution, date and article title.

Submission of a manuscript implies: that the work described has not been published before (except in the form of an abstract or as part of a published lecture, or thesis) that it is not under consideration for publication elsewhere; that if and when the manuscript is accepted for publication, the authors agree to automatic transfer of the copyright to the publisher.

Disclaimer of Warranties

In no event shall Academic Journals be liable for any special, incidental, indirect, or consequential damages of any kind arising out of or in connection with the use of the articles or other material derived from the IJPS, whether or not advised of the possibility of damage, and on any theory of liability.
This publication is provided "as is" without warranty of any kind, either expressed or implied, including, but not limited to, the implied warranties of merchantability, fitness for a particular purpose, or non-infringement. Descriptions of, or references to, products or publications does not imply endorsement of that product or publication. While every effort is made by Academic Journals to see that no inaccurate or misleading data, opinion or statements appear in this publication, they wish to make it clear that the data and opinions appearing in the articles and advertisements herein are the responsibility of the contributor or advertiser concerned. Academic Journals makes no warranty of any kind, either express or implied, regarding the quality, accuracy, availability, or validity of the data or information in this publication or of any other publication to which it may be linked.

International Journal of Physical Sciences

Table of Contents: Volume 8 Number 35 23 September, 2013

ARTICLES

academicJournals

Vol. 8(35), pp. 1738-1745, 23 September, 2013
DOI: 10.5897/IJPS2013.3902
ISSN 1992 - 1950 © 2013 Academic Journals
http://www.academicjournals.org/IJPS

International Journal of Physical Sciences

Full Length Research Paper

Plasma properties of nano-second laser ablated iron target in air

Muhammad Salik[1], Muhammad Hanif [2]*, Jiasheng Wang[1] and Xiqing Zhang[1]

[1]Institute of Optoelectronics, Beijing Jiaotong University, Beijing, China.
[2] MCS, National University of Sciences and Technology, Rawalpindi, Pakistan.

Accepted 9 September, 2013

In the present work, we studied the optical emission spectra of iron (Fe) plasma produced by the fundamental (1064 nm) and second (532 nm) wavelengths of an Nd: YAG laser. The plasma emission has been recorded spatially using five spectrometers covering the spectral region from 200 to 720 nm. The laser beam was focused on target material by placing it in air at atmospheric pressure. The experimentally observed line profiles of neutral iron (Fe I) have been used to extract the electron temperature using the Boltzmann plot method, whereas, the electron number density has been determined from the Stark broadening. The electron temperature is calculated by varying distance from the target surface along the line of propagation of plasma plume and also by varying the laser irradiance. Besides we have studied the variation of number density as a function of laser irradiance as well as its variation with distance from the target surface. It is observed that electron temperature and electron number density increases as laser irradiance is increased.

Key words: Iron, laser ablation, optical emission spectroscopy, electron temperature, electron number density.

INTRODUCTION

The analytical technique employed in this study is Laser-induced breakdown spectroscopy (LIBS), which was first reported by Maker et al. (1964) and has been reviewed by several researchers (Radziemski and Cremers, 1989). This technique is based on optical detection of certain atomic and molecular species by monitoring their emission signals from the laser induced plasma, and provides a useful method to determine the chemical composition of a wide range of materials (Griem, 1997). A LIBS is a simple analytical technique as compared to many other types of elemental analysis because of its straightforward experimental set-up (Miziolek, 2006). It requires a pulsed laser for generating micro-plasma on the target surface and elemental analysis is accomplished by studying the emission of the plasma plume (Cremers and Radziemski, 2007). The laser induced plasma characteristics depend upon several parameters, which include the features of the target, properties of the ambient medium, laser wavelength and pulse duration, etc. (Singh and Thakur, 2007). The element of iron being a good metal and have number of applications in engineering remained in focus by many researchers for long. After the invention of laser and developments in LIBS, many researchers have studied iron plasma in different aspects. Plasma plume photography and spectroscopy of Fe-oxide materials were reported by Viskup et al. (2009). Nanotechnology, nanotoxicology and neuroscience were reported by Suh et al. (2009). Stehrer et al. (2009) discussed the Laser induced breakdown spectroscopy of iron oxide powder. Two dimensional time-resolved x-ray diffraction study of dual phase rapid solidification in steels was reported by

*Corresponding author. E-mail: drhanif-mcs@nust.edu.pk, Fax: +92-51-9270283.

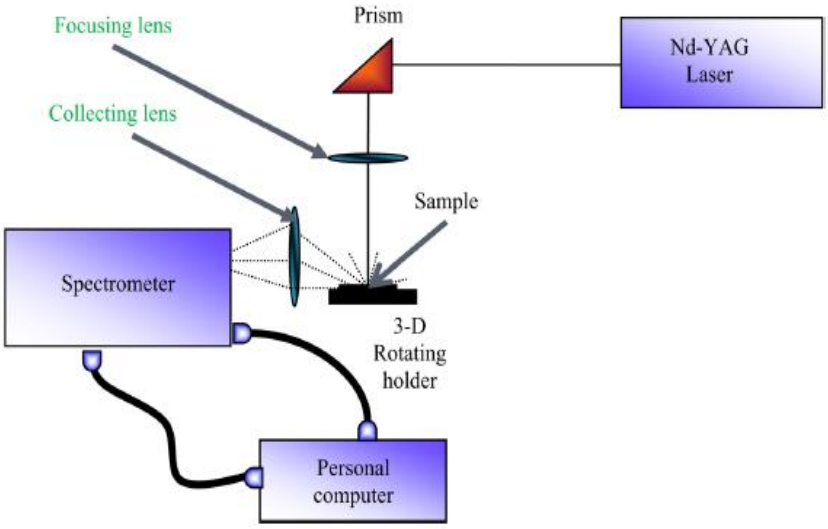

Figure 1. (Color online) Block diagram of the experimental setup.

Mitsuharu et al. (2010). Aswathy et al. (2010) studied an overview on iron based superconductors. Laser cladding of featureless iron-based alloy was discussed by Aghasibeig and Fredrikson (2012). Room temperature ferromagnetic multilayer thin film based on indium oxide and iron oxide for transparent spintronic applications was discussed by Gupta et al. (2010). Plasma nitriding process by direct current glow discharge at low temperature increasing the thermal diffusivity of AISI 304 stainless steel was studied by Prandel et al. (2013). Pulsed laser deposition assisted fabrication and characterization of Fe–Co nanoparticles embedded in Ti N thin film matrix was reported by Kumar et al. (2013). Gautier et al. (2013) recently studied the recent advances in theranostic nanocarriers of doxorubicin based on iron oxide and gold nanoparticles. In the present work, we have studied the spatial evolution of the iron plasma produced by the first (1064 nm) and second (532 nm) wavelengths of a pulsed Nd: YAG laser. The experimentally observed line profiles of neutral iron (Fe I) have been used to extract the electron temperature (T_e) using the Boltzmann plot method, whereas, the electron number density (N_e) has been determined from the Stark broadening. Beside we have studied the variation of electron temperature and electron number density as a function of laser energy at atmospheric pressure.

EXPERIMENTAL DETAILS

The experimental setup is shown in Figure 1 and is same as that described in our previous work (Hanif et al., 2013a, b). Briefly we used a Q-switched Nd: YAG (Quantel Brilliant) pulsed laser having pulse duration of 5 ns and 10 Hz repetition rate which is capable of delivering 400 mJ at 1064 nm, and 200 mJ at 532 nm. The laser pulse energy was varied by the flash lamp Q-switch delay through the laser controller, and the pulse energy was measured by a Joule meter (Nova - Quantel 01507). The laser beam was focused on the target using convex lens of 20 cm focal length. In the experiment, the sample studied was Iron powder containing mass percentage of 99.70% in the sample. A small amount of it was used to prepare a pallet of 15 mm diameter and 3 mm thickness with the help of hydraulic press machine using a load of 10-ton, for a time duration of 5 min. The sample was mounted on a three dimensional sample stage, which was rotated to avoid the non-uniform pitting of the target. The distance between the focusing lens and the sample was kept at 18.5 cm, less than the focal length of the lens to prevent any breakdown of the ambient air in front of the target. The spectra were obtained by averaging 10 data of single shot under identical experimental conditions. The radiation emitted by the plasma were collected by a fiber optics (high-OH, core diameter: 600 μm) having a collimating lens (0 - 45° field of view) placed at right angle to the direction of the laser beam. The optical fiber was connected with the LIBS - 2000 detection system (Ocean Optics Inc.), to measure the plasma emission. The emission signal was corrected by subtracting the dark signal of the detector through the LIBS software. The LIBS - 2000 detection system is equipped with five spectrometers each having slit width of 5 μm, covering the range between 220 - 720 nm. Each spectrometer has 2048 element linear CCD array and an optical resolution of ≈ 0.05 nm by scanning a narrow bandwidth dye laser. In the experiments, the time delay between the laser pulses and the start of the data acquisition is about 3.5 μs, whereas the system integration time is about 2.1 ms and stored by the OOI LIBS software. In order to record the emission spectrum, the LIBS - 2000 detection system was synchronized with the Q-switch of the Nd: YAG laser. The flash lamp out of the Nd: YAG laser triggered detection system through a four-channel digital delay/Pulse generator (SRS DG 535). The LIBS - 2000 detection system triggered the Q-switch of the Nd: YAG laser. The data acquired simultaneously by all the five spectrometers were stored on a PC through the OOILIBS software for subsequent analysis.

RESULTS AND DISCUSSION

In the presented work, we have generated iron plasma using fundamental (1064 nm) and second (532 nm)

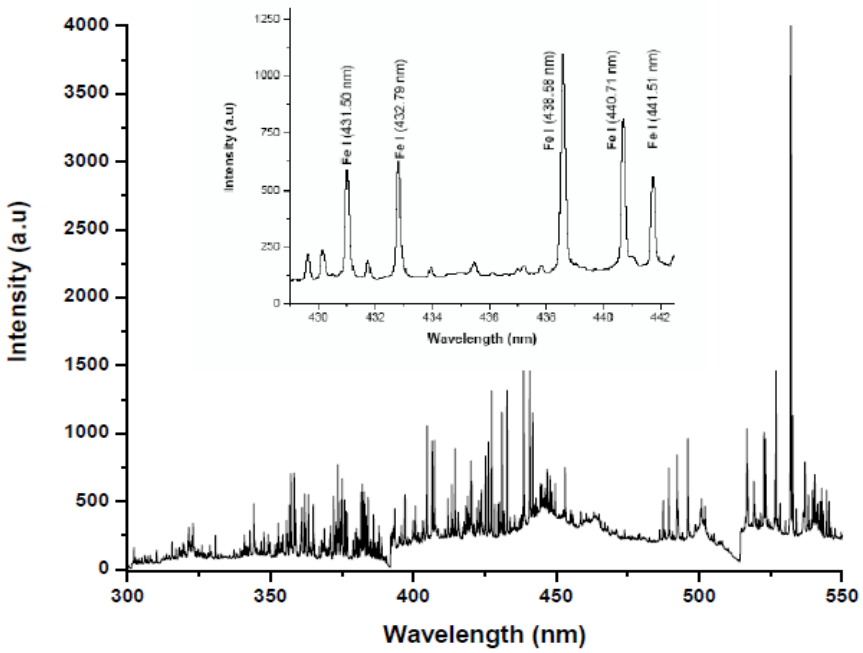

Figure 2. The emission spectrum of neutral iron plasma produced by the second (532 nm) wavelength of the Nd: YAG laser at a distance of 0.05 mm from the target.

Table 1. Spectroscopic parameters of the neutral iron lines used for the determination of plasma parameters.

S/N	Wavelength λ (nm)	Transitions	Statistical weight		Transition probability A_{ki} (s^{-1})	Energy (cm^{-1})	
			g_k	g_i		E_i	E_k
1	431.50	$6p6d\ ^3D_1 \rightarrow 6P^2\ ^3P_0$	5	5	7.7×10^6	17726.981	40894.986
2	432.79	$6p7d\ ^3D_2 \rightarrow 6P^2\ ^3P_1$	5	9	7.9×10^5	26627.604	49726.977
3	440.47	$6p7d\ ^3F_3 \rightarrow 6P^2\ ^3P_2$	7	7	1.3×10^7	29056.321	51837.240
4	438.58	$6p7s\ ^1P_1 \rightarrow 6P^2\ ^3P_1$	9	7	2.75×10^7	12560.930	35257.319
5	441.51	$6p7d\ ^3F_2 \rightarrow 6P^2\ ^3P_2$	7	5	1.19×10^7	12968.549	35611.619

wavelengths of a Q-switched Nd: YAG laser. In the first set of experiments, the fundamental (1064 nm) harmonic laser having 400 mJ pulse energy, and 5 ns pulse width, was focused on the sample target placed in air at atmospheric pressure. The emission spectra of the plasma produced at the surface of the iron target is recorded at different distances along the direction of expansion of the plume. In the experimental arrangement, the laser was focused on the target surface; that is, perpendicular to the target surface, whereas, the plume emission was registered as a function of the distance parallel to the surface of the target material for the spectral region from 200 to 720 nm. Figure 2 shows the window of emission spectrum of iron plasma covering the spectral region from 300 to 550 nm, while the small window in same diagram shows the lines that we used for the determination of electron temperature. All the observed lines in the investigated spectral region along with their assignments are listed in Table 1, based on the data by (Moore, 1971) and listed in the NBS Tables (http://physics.nist.gov).

After observing the well-resolved multiplet structure from a number of excited levels and decaying to a common lower level, it is tempting to extract the plasma parameters from the observed spectra; in particular, the electron number density and the plasma temperature. The electron temperature is determined using the Boltzmann plot method from the relative intensities of the observed line. The following relation has been used to extract the plasma temperature using the formula (Griem 1997):

$$\ln\left(\frac{I_{ki}\lambda_{ki}}{A_{ki}g_k}\right) = \ln\left(\frac{N(T)}{U(T)}\right) - \frac{E_k}{kT} \quad (1)$$

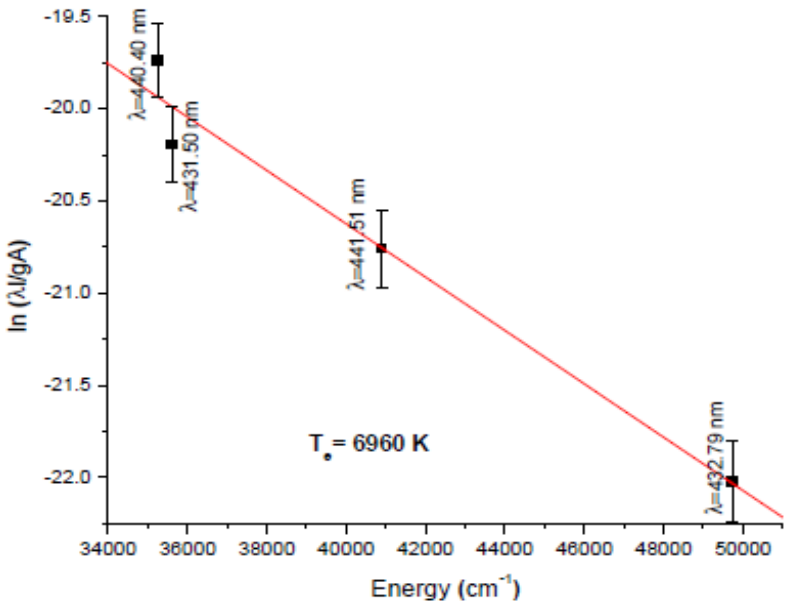

Figure 3. (Color online) Boltzmann plot for the neutral iron spectral lines emitted by the laser induced plasma at 0.0 5 mm from the target at irradiance 4.5×10^{10} W cm^{-2} using the Nd: YAG laser at 532nm.

where, I_{ki} is the integrated line intensity of the transition involving an upper level (k) and a lower level (i), λ_{ki} is the transition wavelength, A_{ki} is the transition probability, g_k is the statistical weight of level (k), $N(T)$ is the total number density, $U(T)$ is the partition function, E_k is the energy of the upper level, k is the Boltzmann constant and T is the excitation temperature. A plot of ln $(\lambda I/gA)$ versus the term energy E_K gives a straight line with a slope equal to $(-1/KT)$. Thus the electron temperature can be determined without the knowledge of the total number density or the partition function. The line identifications and different spectroscopic parameters such as wavelength (λ_{ki}), statistical weight (g_k), transition probability (A_{ki}) and term energy (E_k) are listed in Table 1.

Four neutral iron (Fe I) lines at 431.50, 432.79, 440.47 and 441.51 nm are used for the determination of electron temperature through Boltzmann plot method. These transitions are selected as they have the greatest difference between their corresponding upper energy levels to make the Boltzmann plot more meaningful and to determine electron temperature more accurately. Errors are bound to be present in the determination of the electron temperature by this method, therefore; it is determined with ≈15% uncertainty, coming mainly from the transition probabilities and the measurement of the integrated intensities of the spectral lines.

Figure 3 shows the Boltzmann plot considering the data of all the observed iron lines recorded at (0.05 mm) from the surface of the plasma plume. The line which passes through the data points is a linear fit of above relation (1). The behavior of electron temperature has been studied as function of distance from the target surface for the plasma produced by both modes of the laser. The electron temperature near the target surface is found to be higher and it varies from 7250 to 6850 K from the plasma produced by the first (1064 nm) wavelength of the laser, whereas, in case of second (532 nm) wavelength of the laser, it varies from 6980 to 6500 K over a distance range from 0.05 to 2.0 mm as shown in the Figure 4. The region near the surface of the target material constantly absorbs radiation during the time interval of the laser pulse, causing a higher temperature near the target surface.

One of the most reliable techniques to determine the electron number density is from the measured Stark broadened line profile of an isolated line of either neutral atom or singly charge ion. The electron number density (N_e) related to the full width at half maximum (FWHM) of the Stark broadening lines is given by the relation (Griem, 1997; Cremers and Radziemski, 2007; Singh and Thakur, 2007):

$$\Delta\lambda_{1/2} = 2\omega\left(\frac{N_e}{10^{16}}\right) + 3.5A\left(\frac{N_e}{10^{16}}\right)^{1/4}\left[1-\frac{3}{4}N_D^{-1/3}\right]\omega\left(\frac{N_e}{10^{16}}\right) \quad (2)$$

Where, ω is the electron impact width parameter, A is the ion broadening parameter, N_e is the electron number density and N_D is the number of particles in the Debye sphere. The first term in Equation 2 refers to the broadening due to the electron contribution, whereas, the second term is attributed to the ion broadening. Since the contribution of the ionic broadening is normally very

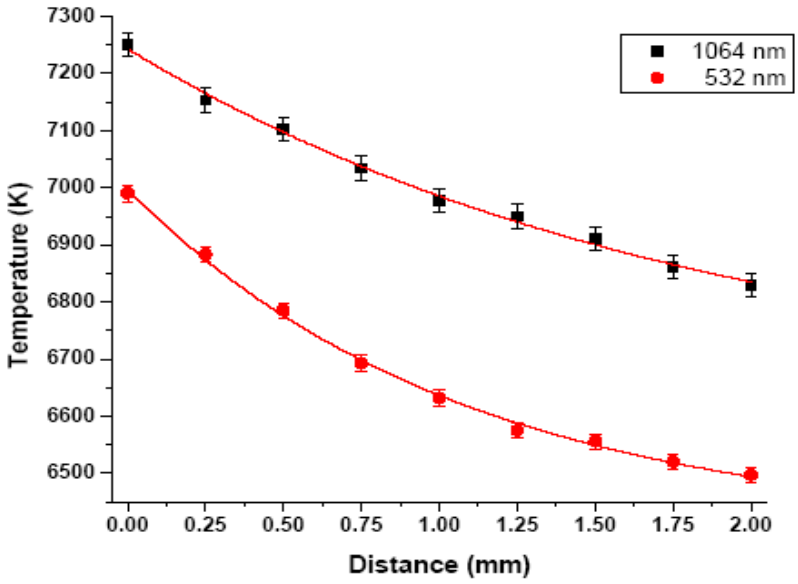

Figure 4. (Color online) variation of the electron temperature along the direction of propagation of the plasma plume using fundamental (1064 nm) and second (532 nm) wavelengths of Nd: YAG laser.

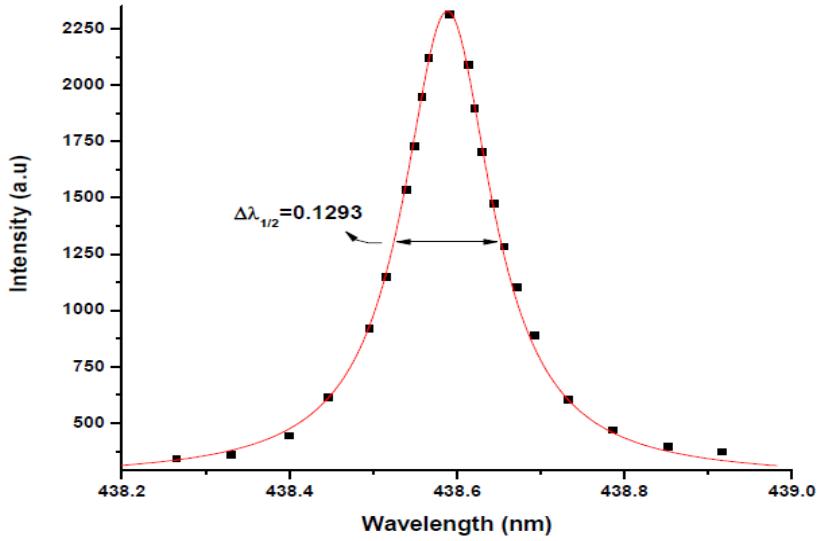

Figure 5. (Color online) Stark broadening profile of neutral iron line at 438.58 nm. The dots represent the experimental profile and the solid line is Lorentizion fit at a distance of 0.05 mm from the target.

small, therefore, it can be neglected and Equation 2 reduced to:

$$\Delta\lambda_{1/2} = 2\omega\left(\frac{N_e}{10^{16}}\right) \quad (3)$$

Here $\Delta\lambda_{1/2}$ is the width of the spectral line, ω is the electron impact broadening parameter and N_e is the electron number density. The value of ω corresponding to different electron temperatures is obtained from the reference data (Griem, 1997). The electron number densities have been determined from the line profiles of the isolated iron neutral lines at 538.34 nm using Relation 3 and $\Delta\lambda_{1/2}$ is extracted by fitting the Lorentzian line shape to the observed data.

Figure 5 shows the line profile of the neutral iron line at 438.50 nm recorded from the plasma, along with the least squares fit of a Lorentizion line shape which yields the width $\Delta\lambda_{1/2}$ of this line. The condition that the atomic

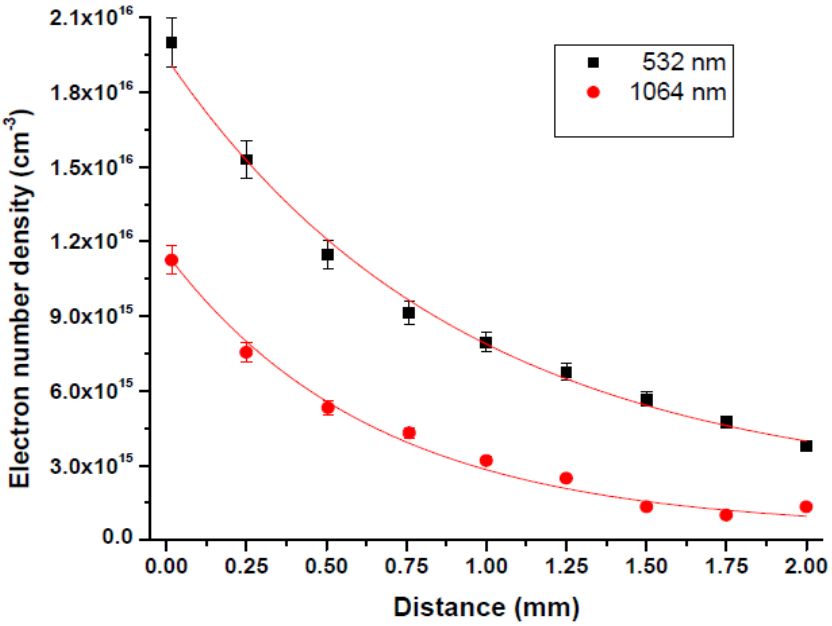

Figure 6. (Color online) Variation of the electron number density with the distance using the fundamental (1064 nm) and second (532 nm) wavelengths of Nd: YAG laser.

states should be populated and depopulated predominantly by electron collisions, rather than by radiation, requires an electron density which is sufficient to ensure the high collision rate. The corresponding lower limit of the electron density is given by the Mc Whirter criterion (Mc Whirter, 1965) to check the condition for the validity of the local thermodynamic equilibrium (LTE):

$$N_e \geq 1.6 \times 10^{12}\ \mathrm{T}^{1/2} (\Delta E)^3 \qquad (4)$$

Here T *(K)* is the plasma temperature and *ΔE (eV)* is the energy difference between the states, which are expected to be in LTE. At ~7000 K, Equation 4 yields $N_e \approx 1.6 \times 10^{14}$ cm^{-3}. The electron number densities determined in our experiments are higher than the required number density which satisfies the LTE condition. Figure 6 shows the number densities for both wavelengths of the laser. The values of number densities using fundamental and second harmonic of the Nd: YAG laser with laser irradiance 6.5 $x10^{10}$ W cm^{-2} are determined as 1.12 x 10^{16} and 2 x 10^{16} cm^{-3} respectively. These values decrease to 1.38 x 10^{15} and 3.75 x 10^{15} cm^{-3} over distance ranges from 0.05 to 2.0 mm from the target surface respectively for neutral iron line at 538.34 nm. The decrease in the number density at large distance is mainly due to the recombination of electrons and ions. As is evident from the Figures 4 and 6, the electron temperature and the electron number density both close to the target are maxima, since the r egion close to the surface continuously absorbs the laser radiation during the laser pulse. When the plasma expands, it thermalizes by transferring the energy to its surroundings and is transparent to the laser pulse; therefore, both plasma parameters decrease along the direction of expansion of the plume. Moreover, the electron temperature and number density decrease rapidly within a short distance from the target surface, while at a large distance, they exhibit little variation. The variation in the electron temperature is slower as compared to that of number density. The internal energy of the plasma is distributed in its thermal and ionization energy. The particle density in the plasma depends on the degree of ionization, evaporation rate and the plasma expansion velocity. Because of the high expansion velocity of the leading plasma edge, the electron density decreases, makes the plasma transparent to the laser beam at larger distance away from the target surface. The absorption in the plasma mainly occurs by an inverse bremsstrahlung and photo ionization process.

In the second set of experiments, we have determined the electron temperature and electron number density for different values of the fundamental (1064 nm) and second (532 nm) wavelengths of Nd: YAG laser. It is observed that the intensities and widths of the spectral lines increase with the increase in the laser irradiance. Figure 7 shows the variation of the electron temperature for the fundamental (1064 nm) and second (532 nm) wavelengths of the laser produced plasma with respect to the laser irradiance at which the temperature varies

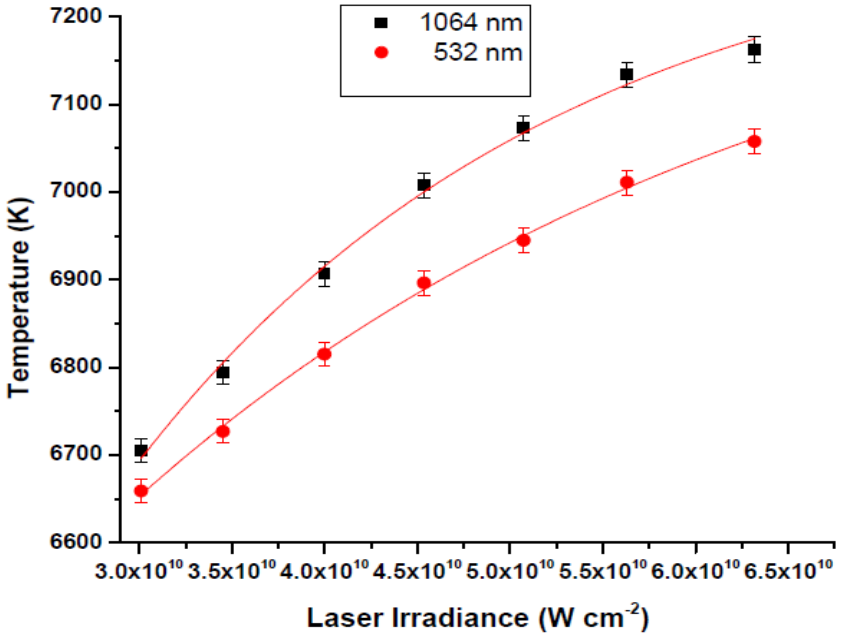

Figure 7. (Color online) Variation of the electron temperature with the laser irradiance using second (532 nm) wavelength of Nd: YAG laser at a distance of 0.05 mm from the target.

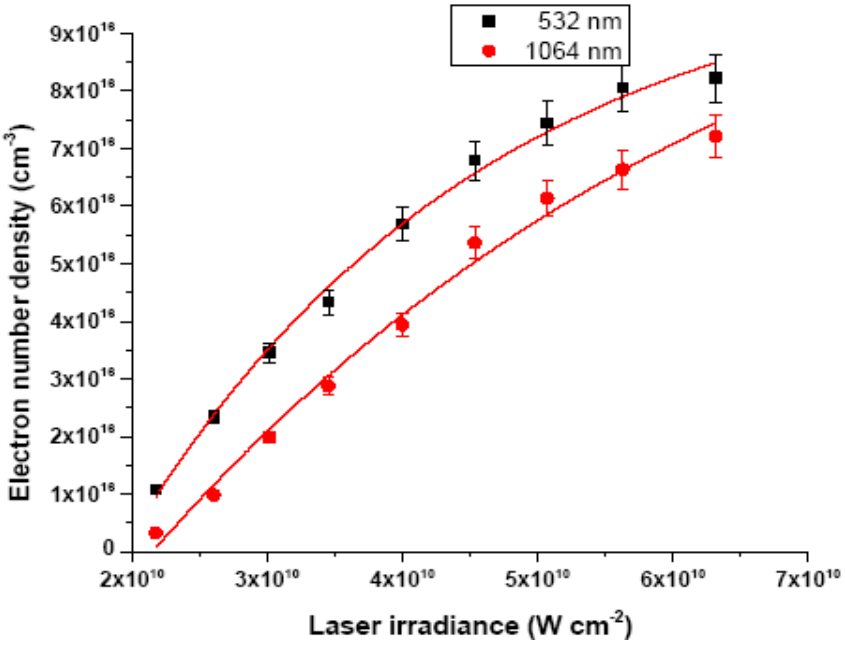

Figure 8. (Color online) Variation of the electron number density with the laser irradiance using first (1064 nm) wavelength of Nd: YAG laser at a distance of 0.05 mm from the target.

from 7165 to 6705 K and from 7060 to 6660 K at a distance of 0.05 mm from the target surface respectively. Evidently, the electron temperature increases with the increase in the laser irradiance. Figure 8 shows the variation in the electron number density as a function of the laser irradiance in case of fundamental (1064 nm)

and second (532 nm) wavelengths of the laser. The variation in the electron number density with the laser irradiance also shows a similar behaviour. The irradiance varies from 6.50 x 10^{10} to 7.25 x 10^{10} watt cm^{-2}, whereas electron number densities vary from 3.29 x 10^{15} to 7.22 x 10^{16} cm^{-3} and 1.08 x 10^{15} to 8.22 x 10^{16} cm^{-3} for fundamental (1064 nm) and second (532 nm) wavelengths of the laser respectively. The increase in the plasma temperatures and electron number densities vary slowly, this may be attributed to the plasma shielding. The observed increase in plasma parameters (N_e and T_e) by the increase of the laser energy is due to the absorption and/or reflection of the laser photon by the plasma, which depends upon the plasma frequency. In our experiment, the corresponding frequency is 2.8 x 10^{14} Hz, whereas the plasma frequency is ν_p= 8.9 x10^3 $\sqrt{Ne}$. The electron number density is $N_e \approx 10^{15}$ cm^{-3}, therefore, ν_p = 3.6 x10^{12} Hz which is less than the laser frequency ($\approx 10^{14}$ Hz), which shows that the energy loss due to the reflection of the laser radiation from the plasma is insignificant.

Conclusion

The LIBS method has been successfully applied as an analytical technique for the analysis of iron plasma using the fundamental (1064 nm) and second (532 nm) harmonics of an Nd: YAG laser. We have determined the electron temperature and the electron number density along the axial position of the plume. It is observed that the spatial behaviour of the electron temperature close to the target is maximum and decreases along the distance from the target, whereas the electron number density close to the target is maximum and decreases as 1/d. Variations of the electron temperature and the electron number density with the laser irradiance shows that both these parameters increase with the increase of the laser irradiance. The values of the plasma parameters (N_e and T_e) determined are well within the range as reported in the previous literature.

REFERENCES

Aswathy PM, Anooja JB, Sarun PM, Syamaprasad U (2010). Topical Review: An overview on iron based superconductors. SuperconD. Sci. Tech. 23:073001-073020.

Aghasibeig M, Fredriksson H (2012). Laser cladding of a featureless iron-based alloy. Surf. Coat. Tech. 209:32-37.

Cremers DA, Radziemski LJ (2007). Handbook of Laser-Induced Breakdown Spectroscopy: New York: Wiley.

Gautier J, Allard-Vannier E, Munnier E, Souce M, Chourpa I (2013). Recent advances in theranostic nanocarriers of doxorubicin based on iron oxide and gold nanoparticles. J. Controlled Release 169:48–61.

Griem HR (1997). Principles of Plasma Spectroscopy: Cambridge University Press. 10.1017/CBO9780511524578.

Gupta RK, Ghosh K, Kahol PK (2010). Room temperature ferromagnetic multilayer thin film based on indium oxide and iron oxide for transparent spintronic applications. Mater. Lett. 64:2022–2024.

Hanif M, Salik M, Baig MA (2013a).Optical spectroscopic studies of titanium plasma produced by an Nd: YAG Laser. Opt. Spectrom. 114:7-14.

Hanif M, Salik M, Sheikh MN, Baig MA (2013b). Laser-based optical emission studies of barium plasma. Appl. Phys. B: Lasers Optics 110:563-571.

Kumar D, Sarin A, Verma V, Venkatraman R (2013). Pulsed laser deposition fabrication and characterization of Fe–Co nanoparticles embedded in TiN thin film matrix. Thin Solid Films 534:561–565.

Maker PD, Terhune RW, Savage CM (1964). Quantitative Electronics, Proceedings of the 3rd International Conference: Columbia University Press, New York.

Mc Whirter RWP (1965). Plasma diagnostic techniques. New York: Academic Press.

Mitsuharu Y, Takahiro O, Hidenori T, Yuichi K, Masugu S, Hidenori, Akiko N (2010). Two-dimensional time-resolved x-ray diffraction study of dual phase rapid solidification in steels. J. Appl. Phys. 107: 013523-013523-6.

Moore CE (1971). Atomic Energy Levels, NBS circular No. 467, Washington DC.

Miziolek AW, Palleschi V, Schechter I (2006). Laser-induced breakdown spectroscopy (LIBS): Fundamentals and applications. Cambridge University Press.

Prandel L, Somer V, Assmann A, Camelotti A, Costa F, Bonardi G, Jurelo C, Rodrigues AR, Cruz GK (2013). Plasma nitriding process by direct current glow discharge at low temperature increasing the thermal diffusivity of AISI 304 stainless steel. J. Appl. Phys. 113: 063507-063507-5.

Radziemski LJ, Cremers DA (1989). Laser-induced plasma and applications. New York.

Singh JP, Thakur SN (2007). Fundamental of Laser-Induced Breakdown Spectroscopy: Elsevier B.V.

Stehrer T, Praher B, Viskup R, Jasik J, Wolfmeir H, Arenholz E, Heitz J, Pedarnig JD (2009). Laser-induced breakdown spectroscopy of iron oxide powder. J. Anal. At. Spectrom. 24:973-978.

Suh WH, Stucky GD, Suh YH (2009). Nanotechnology, nanotoxicology and neuroscience. Progress Neurobiol. 87:133-170.

Viskup R, Praher B, Stehrer T, Jasik J, Wolfmeir H, Arenholz E, Pedarnig JD, Heitz J (2009). Plasma plume photography and spectroscopy of Fe-oxide materials. Appl. Surf. Sci. 255:5215-5219.

academicJournals

Vol. 8(35), pp. 1746-1752, 23 September, 2013
DOI: 10.5897/IJPS2013.3955
ISSN 1992 - 1950 © 2013 Academic Journals
http://www.academicjournals.org/IJPS

International Journal of Physical Sciences

Full Length Research Paper

Wavelet based dynamic Mel Frequency Cepstral Coefficients (MFCC) and block truncation techniques for efficient speaker identification under narrowband noise conditions

S. Selva Nidhyananthan*, R. Shantha Selva Kumari and D. S. Roland

Department of ECE, Mepco Schlenk Engineering College, Sivakasi-626005, India.

Accepted 09 September, 2013

Speaker identification strategies are well convincing in their performance when clean speeches are scrutinized. But the performance degrades when speech samples are corrupted by narrowband noise. Block truncation of the cepstral coefficients ensures that not all the features are affected by narrowband noise but it cannot reduce the extent of degradation. This work is focused towards improving the performance of speaker identification systems by block truncating the features which are subjected to wavelet processing. Wavelet decomposition divides the entire energy spectrum of the speech signal into bands corresponding to the number of levels of decomposition performed in the wavelet transformation thereby segregating the noise affected bands from other bands. In addition to that, wavelet filters provide the smoothening of the noisy speech signals which enhances the identification of the correct speaker. Dynamic Mel filtering of these wavelet coefficients followed by block truncation provides better identification, taking advantage of the fact that some filter bank coefficients remain unaffected by narrowband noise. The features are modeled by Gaussian mixture model - Universal background model (GMM-UBM) that serves as a generic one timed trained model. Speaker identification efficiency of 97.23% is achieved through this wavelet based dynamic MFCC technique which exhibits 7.58% improvement in speaker identification accuracy when compared with non wavelet based block truncation method.

Key words: Wavelet decomposition, block truncation, Dynamic Mel Filtering Cepstral Coefficients (DMFCC), Gaussian mixture model - Universal background model (GMM-UBM), speaker identification.

INTRODUCTION

Speaker identification is a biometric process (ZoranCirovi et al., 2010) of identifying a person by comparing the features extracted from the person to be identified, with the features extracted from the speakers enrolled in the database. The success of speaker identification depends upon the feature extracted and its modeling method (Campbell, 1997). The feature extracted during testing phase will match the feature extracted during enrollment phase perfectly, if the conditions under which it is tested are ideal. But under practical circumstances the testing conditions will include noise disturbances such as car noise, train noise, narrowband noise, etc. The car and train noises can be thought of disturbances that degrade the performance effectively depending upon the signal to noise ratio.

*Corresponding author. E-mail: nidhyan@mepcoeng.ac.in, Tel.:+91-4562-235409, Fax: +91-4562-235111.

Abbreviations: MFCC, Mel Frequency Cepstral Coefficients; **UBM**, Universal Background Models; **DCT**, Discrete Cosine Transform; **MFLE**, Mel Filter Log Energies.

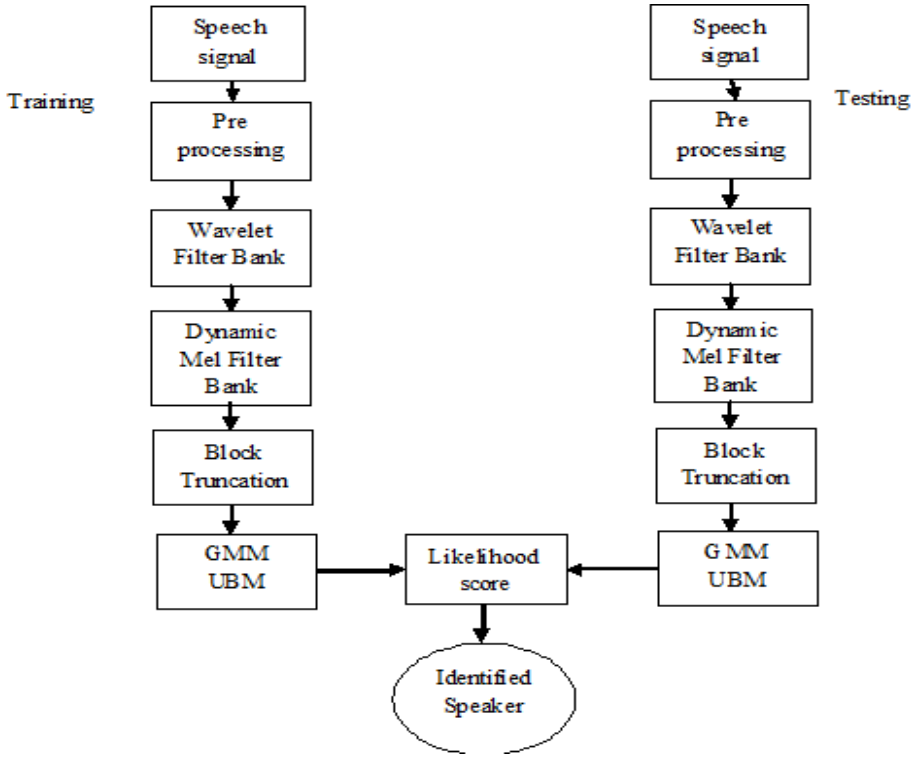

Figure 1. Overall block diagram of the proposed speaker identification system.

Moreover, the testing environments with these conditions are usually avoided in the practical speaker identification circumstances. But the narrowband noises are short time disturbances that are present in almost all the testing environments which lead to performance degradation of the speaker identification system. This problem can be overcome by a strategy called block based transformation, which is detailed in Sahidullah and Saha (2011).

The most common feature used for speaker identification is Mel Frequency Cepstral Coefficients (MFCC). As the human auditory system is most sensitive to the pitch frequency of the speaker, a feature that is based on the pitch frequency will model the speaker much more efficiently than the features that are not based on the pitch frequency of the speaker. In this work, Dynamic Mel Frequency Cepstral Coefficients (DMFCC) are used as features, which are formed by imparting the pitch frequency into the MFCC thereby producing dynamic features. The feature extracted is then used to model the speaker by using Universal Background Models (UBM). But the problem in modeling is that whether the model adapts itself for all the speakers enrolled in the database or not. This is called the bias/ variance dilemma problem (Utpal and Kshirod, 2012).

The Discrete Cosine Transform (DCT) is popularly used for MFCC and DMFCC computation, because the correlation matrix of Mel Frequency Log Energy data is similar to the correlation matrix of first order Markov process and DCT provides better energy compaction (Kekre and Vaishali, 2011) than any other linear transform. In this work, DCT is carried out in blocks to mitigate the effects of narrowband noise since the effect of a noise corrupted Mel Filter Log Energies (MFLE) will not pronounce in the MFCC obtained through other DCT blocks. Therefore by combining the narrowband noise overcoming strategies (Qi and Yan, 2011) of Block Truncated DCT and sub band processing, together with the added advantage of eliminating the bias / variance dilemma by sub band concept, enhanced speaker identification can be obtained. TIMIT database has been used in this work. The speeches in TIMIT database (John et al., 2013) was recorded at TI, transcribed at MIT and produced by the National Institute of Standards and Technology (NIST). The TIMIT database consists of 630 speakers.

This paper focuses on segregating the noise affected portions of speech, by making blocks of speech frames to confine the noise spread using wavelet transform, which reduces the effects of noise degradation when higher levels of decomposition is performed.

PROPOSED SYSTEM

The overall block diagram representing the speaker identification system is shown in Figure 1. The speech signal is first pre-processed and the energy spectrum of the speech wave is

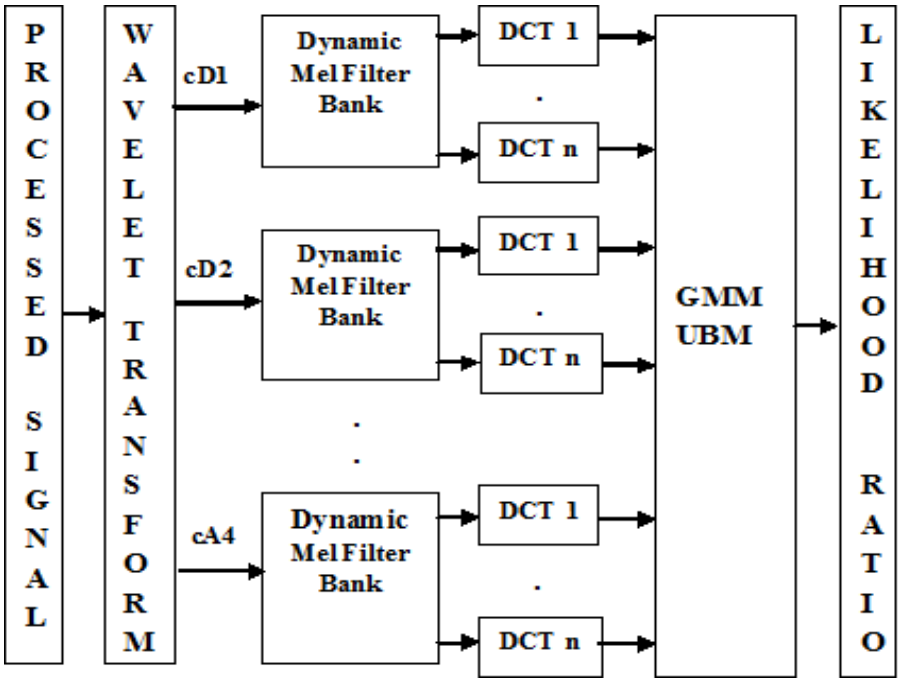

Figure 2. Block diagram of wavelet processed DMFCC.

computed using multilevel wavelet decomposition. The wavelet transformation divides the spectrum into appropriate number of bands corresponding to the number of levels of decomposition performed in the transformation. The wavelet filter outputs are robust to noise degradation due to the smoothening effect of the low pas filters while performing the discrete wavelet transformation on the speech signal. Moreover, the wavelet filter bank acts as dividing the entire bandwidth of the speech signal into bands corresponding to the number of levels used in the wavelet transformation. Moreover, the noise affected band is confined to one or few bands rather than being available at the whole spectrum. Hence it is easy to process the noise affected sub bands uniquely using Block truncation strategy. The methodology of the proposed work is enhancing the speaker identification under narrowband noise condition which makes the speech signal at 10 dB signal to noise ratio (SNR), by the features extracted through wavelet processing. Wavelet filters provide smoothening of the noise affected speech signal which provides reduction of the degradation caused by noise when higher levels of decomposition is performed on wavelet transformation. Further, the block truncation of the cepstral coefficients helps in restricting the effect of narrowband noise in affecting all the energy coefficients. Hence when the features are modeled using GMM-UBM, improvement in speaker identification accuracy can be achieved. The central schematic of this work lies in the sub band and block truncation techniques which is depicted in Figure 2. Each of these bands of wavelet coefficients is then provided as inputs to individual Dynamic Mel Filter Bank to obtain the Wavelet Dynamic Mel Frequency Cepstral Coefficients (WDMFCC). These features are more robust because the noise affected speech signal is smoothened by the low pass filters of the wavelet transformation process.

The features are then extracted by decorrelating the Dynamic Mel Filter Log Energies using block truncated DCT. Here, instead of taking DCT for the entire log energies of the sub band, DCT is performed in a block truncated manner because when DCT is performed on individual blocks narrowband noise in a block will not spread to the other blocks in the sub band. The features are then used to model the speaker by means of Gaussian Mixture Models-Universal Background Model (GMM-UBM).

Speaker identification steps

Speaker identification process is a kind of pattern classification. In pattern classification problem, the first step is evaluating representation of input pattern. In speaker identification, this step is evaluation of power spectrum. These acoustic representations are extracted within successive analysis windows of 20-30 ms overlapped by 10 ms size. As vocal tract is a slowly varying system, speech signal is nearly stationary over this analysis window. Other pre processing stages are briefly outlined here for the sake of completeness.

Pre-emphasis

Pre-emphasis (Tomi and Haizhou, 2010) is performed to boost the higher frequencies of the signal. It is performed with a pre-emphasis factor of 0.97 according to the equation given by:

$$y(n) = x(n) - \alpha x(n-1) \quad (1)$$

Pre-emphasis offsets the negative spectral slope of 20 dB per decade that is naturally present in the speech signals.

Windowing

The pre-emphasized signal is then segmented into smaller frames for the stationary property to be satisfied in taking DFT. Hamming window (Rabiner and Biing-Hwang, 2007) is used in this work. It is given by:

$$w(n) = 0.54 - 0.46\cos(\frac{2\pi n}{N-1}) \quad ,0 \le n \le N-1 \tag{2}$$

The windowed signal is given by:

$$S_w(n) = y(n) * w(n) \tag{3}$$

where $y(n)$ is the pre-emphasized signal and $w(n)$ is the window used.

Energy spectrum

The energy spectrum of the windowed frames is computed by taking wavelet transform. Wavelet transforms have advantages over traditional Fourier transforms for representing functions that have discontinuities and sharp peaks, and for perfect deconstructing and reconstructing finite, non-periodic and/or non-stationary signals. The transformation is given by:

$$X(k) = \left| DWT(S_w(n)) \right|^2 \tag{4}$$

Wavelet bands

Successful speaker identification is critically dependent on obtaining good speaker models from training data. Data modeling is subjected to the bias/variance dilemma (Vibha and Jyoti, 2011). According to this, models with too many adjustable parameters will tend to overfit the data, exhibiting high variance and hence the model will generalise poorly. On the other hand, few parameters will make the model biased. Wavelet processing (Pawar and Badave, 2011) helps to solve this problem by dividing the entire energy spectrum of the speech signal into bands corresponding to the number of levels performed in the wavelet transformation (Vale and Alcaim, 2008). Also, the low pass filters of the wavelet transformation acts as smoothening filters (Sridhar et al., 2012) thereby reducing the degradation of signal by noise. The wavelet energy coefficients are then fed to the Mel scale filters for extracting speaker specific features.

DMFCC feature extraction

Features are the representatives of the speech signal in speaker identification task. Feature extraction is the estimation of variables, called a feature vector, from another set of variables called speech samples. The feature extraction will transform the speech signal into feature vectors which present the specific properties of each speaker. Raw speech signals cannot be used as such for speaker identification because of two reasons: (i) direct comparison and identification are complex and unreliable and (ii) requires large storage capability.

The human auditory system can sensitively perceive the changes in pitch. The pitch frequency is calculated by taking the autocorrelation of the signal and then taking maximum value for the autocorrelation function. Therefore by incorporating the pitch information into the MFCC feature, dynamic mel frequency cepstral coefficients can be extracted, which proves to provide strong robustness to background noise compared other features (Wang, et al., 2009) thus increasing the identification rate.

$$Mel(f_{ip}) = 2595\log(1 + f_{ip}/700) \tag{5}$$

where f_{ip} is the pitch frequency of i^{th} frame. The Mel frequency energy spectrum is then passed through the Gaussian Mel filter bank (Sandipan and Goutam, 2009) followed by cosine transformation to obtain DMFCC features.

Block truncation transformation

Discrete cosine transform is performed on Dynamic Mel Filter Log Energies (DMFLE) to decorrelate them and so to make the extracted feature suitable for modeling. When such DCT is applied to a narrowband noise affected speech signal's log energies, all the features will be affected by the noise and hence will make it unsuitable for speaker identification. To alleviate this problem, block based transformation is performed. The filter log energies are divided into blocks and DCT is performed on them. This will ensure that a narrowband noise affected block will not pronounce its effect in the feature extracted from the other DMFLE blocks of the speech signal and hence will facilitate correct identification of the speaker. Narrow band noise (Ming et al., 2007) is synthetically generated by adding four frequency components (that is, sinusoidal tones) of 2000, 2100, 2200 and 2300Hz. The amplitudes of the sinusoids are chosen randomly.

The filter bank log energies are decomposed into several blocks unlike standard full band based DCT technique. In this work, the whole signal is divided into non-overlapping blocks (Jingdong et al., 2000) and individual blocks are processed independently. Therefore, the presence of narrowband noise in one block will not affect the other blocks because of truncation. The transformation matrix can be given as:

$$L = \Phi_1 \oplus \Phi_2 \oplus \cdots \oplus \Phi_N = \begin{bmatrix} \Phi_1 & 0 & 0 & \cdot & \cdot & 0 \\ 0 & \Phi_2 & 0 & \cdot & \cdot & 0 \\ \cdot & \cdot & \cdot & \cdot & \cdot & \cdot \\ \cdot & \cdot & \cdot & \cdot & \cdot & \cdot \\ 0 & 0 & 0 & \cdot & \cdot & \Phi_N \\ & & & & & \end{bmatrix} \tag{6}$$

Where $\Phi_1, \Phi_2, \Phi_3 .... \Phi_N$ are orthogonal discrete cosine transformation matrices applied to individual blocks of Dynamic Mel Filter Log Energies (DMFLE).

Suppose two blocks of same sizes q are considered then the DCT matrix of size $q \times (q-1)$ is given by $\phi_1 = \sqrt{\frac{2}{q}} \cos\left[\frac{\pi i(2j+1)}{2q}\right]$ and $\phi_2 = \sqrt{\frac{2}{p-q}} \cos\left[\frac{\pi(i-q)(2j+1)}{2(p-q)}\right]$.

GMM-UBM

A Universal Background Model (UBM) is a model used in a biometric identification system to represent general, person independent feature characteristics to be compared against a model of person-specific feature characteristics. The likelihood ratio statistic is given by:

$$LR(X) = \frac{p(X/\lambda_p)}{p(X/\lambda_{\bar{p}})} \tag{7}$$

where $p(X/\lambda_p)$ is the probability that the feature models the speaker correctly, $p(X/\lambda_{\bar{p}})$ is the probability that the feature belongs to the alternate hypothesis.

$\lambda = \{w_i, \mu_i, \sigma_i\}$, i=1,2,...$M$

M is the number of Gaussian components, w_i is the mixture weights, μ_i is the means and σ_i is the variance.

The alternate hypothesis that gives the probability of speaker belonging to the false category is modeled by means of UBM. It is a speaker independent one time trained model. Since UBM is a large GMM (Reynolds, 1995; Reynolds and Rose, 1995) trained to represent the speaker independent features, its idea is to capture the general characteristics of a population and then adapting it to the individual speaker by means of EM algorithm. With training vectors from the hypothesized speaker, X={ $x_1, x_2 ... x_T$ } and for mixture 'i', the probability distribution is given by:

$$\Pr(i / x_i) = \frac{w_i p_i(x_t)}{\sum_{j=1}^{M} w_j p_j(x_t)} \quad (8)$$

Then with the distribution known, the statistics for the weight, mean, and variance parameters are initialized as given as follows:

$$n_i = \sum_{i=1}^{T} \Pr(i / x_t)$$

$$E_i(x) = \frac{1}{n_i} \sum_{t=1}^{T} \Pr(i / x_t) x_t \quad (9)$$

$$E_i(x^2) = \frac{1}{n_i} \sum_{t=1}^{T} \Pr(i / x_t) x_t^2$$

The updated coefficients are given by:

$$w_i^{new} = [\alpha n_i / T + (1-\alpha) w_i]\gamma$$
$$\mu_i^{new} = \alpha E_i(x^2) + (1-\alpha)\mu_i \quad (10)$$
$$\sigma_i^{2new} = \alpha E_i(x^2) + (1-\alpha(\sigma_i^2 + \mu_i^2)) - \mu_i^{2new}$$

where $\alpha = \frac{n_i}{n_i + r}$ with relevance factor r = 16

RESULTS AND DISCUSSION

TIMIT database is used for the analysis in this speaker identification work. Each speaker record contains ten speech signals, from which six signals are used for training and the remaining four signals are used for testing. The database consists of clean speech recorded at 16 kHz sampling frequency. The maximum frequency content in the speech waveform is 8 kHz. The TIMIT database speech signals are subjected to Narrow band noise generated by adding four frequency components of 2000, 2100, 2200 and 2300 Hz. The narrow band noise affected speech signal is first pre-processed and the energy spectrum of the speech wave is computed using four level decomposed wavelet transformation. Thus energy spectrum is obtained into bands corresponding to the number of decomposition levels. Now the noise affected band is confined to one or few bands rather than being available at the whole spectrum. Hence, it is easy to process the noise affected sub bands uniquely using Block truncation strategy. Since the band processing is done well ahead of decorrelarion step, the narrowband noise affected portion can be segregated from the rest of the bands that are not affected by the noise and better decorrelation is achieved at the Discrete Cosine Transform stage of Dynamic Mel Frequency Cepstral Coefficient feature extraction.

To improve the speaker identification efficiency, Dynamic Mel scale filter bank is constructed using Gaussian shaped filters in contrary to the triangular filters used in conventional systems. A triangular filter provides crisp partitions in an energy spectrum by providing non-zero weights to the portion covered by it while giving zero weight outside it. This phenomena cause loss of correlations between a sub band output and the adjacent spectral components that are present in the other sub band, whereas Gaussian shaped filters can provide much smoother transition from one sub band to other preserving most of the correlation between them. The DMFCC feature thus extracted is modeled using GMM-BUM modeling with 2048 mixture components.

During testing, the percentage of correct identification is calculated by using the formula:

$$Percentage\ of\ correct\ identification = \frac{No.\ of\ \ utterances\ correctly\ identified}{Total\ no.\ of\ utterances\ under\ test} * 100$$

The DMFCC features results have been observed for frame sizes of 1024, 512, and 256 without wavelet decomposition. The identification performance is tabulated in Table 1. The performance deteriorates in full band DCT since the effect of narrowband noise will be spread out to all the filter bank coefficients. But under the pro block based DCT system, the identification rate enhances to 89.65% for a frame size of 256. This proves the advantage of block based transformation under narrowband noise conditions. This accuracy can be further enhanced by the proposed wavelet based DMFCC feature. The WDMFCC features results have been observed for frame sizes of 1024, 512, and 256 with two level wavelet decomposition. The identification performance is tabulated in Table 2.

The percentage of correct identification improves to 94.13% for the frame size of 256. The wavelet filters provides coefficients that represent the smoothened version of the noise affected speech signal which when dynamic mel filtered followed by block truncation, reduces the noise degradation and provides improved identification percentage. Now the WDMFCC features results have been observed for frame sizes of 1024, 512, and 256 with three level wavelet decomposition. The identification performance is tabulated in Table 3. It is inferred from Table 3 that the performance of speaker

Table 1. Identification performance for DMFCC with and without block truncation

S/N	Total number of speakers	GMM-UBM		
		Frame size	Identification accuracy in presence of narrowband noise (%)	
			Without block truncation	With block truncation
1	630	1024	61.57	73.05
2		512	75.25	81.97
3		256	83.73	89.65

Table 2. Identification performance for WDMFCC with and without block truncation for two-level wavelet decomposition

S/N	Total number of speakers	GMM-UBM		
		Frame size	Identification accuracy in presence of narrowband noise (%)	
			Without block truncation	With block truncation
1	630	1024	71.13	82.88
2		512	80.50	87.25
3		256	87.21	94.13

Table 3. Identification performance for WDMFCC with and without block truncation for three level wavelet decomposition

S/N	Total number of speakers	GMM-UBM		
		Frame size	Identification accuracy in presence of narrowband noise (%)	
			Without block truncation	With block truncation
1	630	1024	72.75	83.5
2		512	81.13	88.38
3		256	88.25	96.37

identification system is improved to 96.37% corresponding to frame size of 256. The improvement corresponds to the higher level decomposition of the wavelet transformation which exhibit better noise smoothening compared to the results obtained through two level wavelet processed DMFCC results.

The identification performance for WDMFCC features with four level wavelet decomposition for frame sizes of 1024, 512, and 256 is tabulated in Table 4. From Table 4, it is observed that the identification accuracy is improved to 97.23% for the Dynamic Mel features obtained through four-level wavelet decomposition. The accuracy is enhanced by 7.58%. The results are compared with (Ramaligeswararao et al., 2011) the work on text-independent speaker identification model is developed by integrating MFCC's with Independent component analysis (ICA) for obtaining feature independency and to achieve low dimensionality in feature vector extraction. The work by Ramaligeswararao et al. (2011) evaluated the speaker identification performance for a database of 50 speakers under 0dB, 10dB and 20 dB SNR conditions and obtained a maximum identification performance of 72.34% for 10 dB SNR and 88.45% for 20 dB SNR. But our proposed work achieves 97.23% for 630 speakers even at 10 dB SNR.

Conclusion

In this paper, the speaker identification rate under

Table 4. Identification performance for WDMFCC with and without block truncation for four level wavelet decomposition

S/N	Total number of speakers	GMM-UBM		
		Frame size	Identification accuracy in presence of narrowband noise (%)	
			Without block truncation	With block truncation
1	630	1024	73.62	84.69
2		512	81.63	88.87
3		256	88.50	97.23

narrowband noise conditions is found to be enhanced by the features extracted through wavelet processing. Wavelet filters provide smoothening of the noise affected speech signal which provides reduction of the degradation caused by noise when higher levels of decomposition is performed on wavelet transformation. The block truncation of the cepstral coefficients helps in restricting the effect of narrowband noise in affecting all the energy coefficients. The identification performance stands at 97.23% for the four level wavelet decomposed WDMFCC for a frame size of 256. Further developments such as fusion of several other features with adaptive weights can improve the narrowband noise performance to significant levels of successful identification accuracies.

REFERENCES

Campbell JP (1997). Speaker identification: A tutorial,Proc. IEEE. 85(9):1437-1462.

Kekre HB, Vaishali K (2011). Speaker Identification using Row Mean of DCT and Walsh Hadamard Transform. Int. J. Comput. Sci. Eng. 3(3):1295–1301.

Jingdong CU, Kuldip K, Paliwal K, Nakamura S (2000). A block cosine transform and its application in speech identification. In: Proc Int. Conf. Spoken Language Processing (INTERSPEECH 2000 – ICSLP) IV:117–120.

John HL, Hansen L, Jun-Won S, Matthew RL (2013). In-set/out-of-set speaker recognition in sustained acoustic scenarios using sparse data. Speech Commun. 55(6):769–781.

Ming J, Timothy JH, James RG, Douglas AR (2007). Robust speaker identification in noisy conditions. IEEE Trans. Audio Speech Lang. Process. 15(5):1711–1723.

Ramaligeswararao NM, Sailaja V, Srinivasa R (2011). Text Independent Speaker Identification using Integrated Independent Component Analysis with Generalized Gaussian Mixture Model. Int. J. Adv. Comput. Sci. Appl. 2:12.

Pawar MD, Badave SM (2011). Speaker Identification System Using Wavelet Transformation on Neural Network. Int. J. Comput. Appl. Eng. Sci. I Special Issue on Cns ,July 2011.

Rabiner LR, Biing-Hwang J (2007). Fundamentals of speech Identification. Pearson Education Book.

Reynolds D, Rose R (1995). Robust text-independent speaker Identification using Gaussian mixture speaker models." Speech Audio Process. IEEE Trans. 3(1):72–83.

Reynolds DA (1995). Speaker identification and verification using Gaussian mixture speaker models. Speech Communication.

Sahidullah Md, Saha G (2011). Design, analysis and experimental evaluation of block based transformation in MFCC computation for speaker identification, IEEE.

Sandipan C, Goutam S (2009). Improved Text-Independent Speaker Identification using Fused MFCC & IMFCC Feature Sets based on Gaussian Filter. Int. J. Info. Commun. Eng. 5(1).

Sridhar KN, Dmitry Z, Ramani D, Mounya E (2012). Biomimetic Multi-Resolution Analysis for Robust Speaker Identification EURASIP J. Audio, Speech Music Processing 2012:22 doi:10.1186/1687-4722-2012-22.

Tomi K, Haizhou L (2010). An overview of text-independent speaker recognition: From features to supervectors. Speech Commun. 52:12–40.

Wang Y, Li B, Jiang X, Liu F, Wang L (2009). IEEE April 2009 Speaker Identification based on Dynamic MFCC parameters, pp. 406-409.

Qi L, Yan H (2011). An Auditory-Based Feature Extraction Algorithm for Robust Speaker Identification Under Mismatched Conditions. IEEE Trans. Audio, Speech Lang. Process. 19(6).

Utpal B, Kshirod S (2012). GMM-UBM Based Speaker Verification in Multilingual Environments. Int. J. Comput. Sci. 9(6):2.

Vale E, Alcaim A (2008). Adaptive weighting of subband-classifier responses for robust text-independent speaker identification. Electron. Lett. 44(21):1280–1282.

Vibha T, Jyoti S (2011). Wavelet Based Noise Robust Features for Speaker Recognition. Sig. Process. An Int. J. (SPIJ) 5(2).

ZoranCirovi C, Milan M, Zoran B (2010). Multimodal Speaker Verification Based on Electroglottograph Signal and Glottal Activity Detection. EURASIP J. Adv. Sig. Process. Article ID 930376, p. 8.

academicJournals

Vol. 8(35), pp. 1753-1760, 23 September, 2013
DOI: 10.5897/IJPS2013.3954
ISSN 1992 - 1950 © 2013 Academic Journals
http://www.academicjournals.org/IJPS

International Journal of Physical Sciences

Full Length Research Paper

Performance analysis of a Ĉuk regulator applying variable switching frequency

Md. Nazmul Hasan[1]*, Md. Shamimul Haque Choudhury[1,2], M. Shafiul Alam[1,2] and Muhammad Athar Uddin[1,2]

[1]International Islamic University Chittagong (Dhaka Campus), 147, Green road, Dhaka-1205, Bangladesh.
[2]Bangladesh University of Engineering and Technology, Bangladesh.

Accepted 09 September, 2013

This paper examines the performance of Ĉuk regulator to convert three phase alternating current (ac) to direct current (dc). Firstly, three phase ac is rectified with bridge diode. The rectified dc voltage is applied to input of a Ĉuk regulator. Three phase harmonics filter is introduced at the input of the diode rectifier to improve the shape of the input current. The main technique applied here to improve the performance of the regulator is a variable switching frequency which is applied to the gate of the IGBT; that is, at different duty cycle of the regulator, the switching frequency is different. The total harmonics distortion (THD) of the input current and the efficiency of the regulator are observed. The results shown here are simulated with Pspise.

Key words: Ĉuk regulator, total harmonics distortion (THD), duty cycle.

INTRODUCTION

The demand of high quality power is increasing day by day in both commercial and industrial purpose. A great amount of work has already been done concerning the three-phase pulse width modulation (PWM) boost rectifier (Ooi et al., 1985; Wu et al., 1988; Wu et al., 1991; Habetler, 1993; Blasko and Kaura, 1997) and the buck rectifier (Kataoka et al., 1979; Busse and Holtz, 1982; Wiechmann et al., 1984; Ziogas et al., 1985). The disadvantage of these buck rectifiers is not being capable of providing more voltage than the input voltage. Another technique is boost type, which have the limitation of not being capable of providing output voltage lower than the input voltage. To overcome this limitation, a three phase PWM buck-boost rectifiers has been proposed in (Kikuch and Thomas, 2002). High order harmonic control analysis has been done. Combination of rectification and inversion function increases the complexity of operation and control of the scheme. Pulse generation is difficult because it is divided into three classes which increase difficulty of implementation. But, simplicity is a high consideration to design a regulator. Moreover, input current was found very high and no analysis has been reported to reduce the input current. A Ĉuk regulator was also proposed (Ruma, 2008) to improve the quality of the input current. This allows both steps up and step down control of rectifier output voltage. However, the study did not provide solution to input currents worsening shape with voltage control by duty cycle change. A switch mode regulator based on Ĉuk principle has been presented in (Alomgir, 2005) to regulate ac voltage to a desired value irrespective of the input voltage and load. But the efficiency was poor and no analysis has been done to improve input current. An improved voltage regulator and three phase rectifier based on boost topology are proposed in (Ahmed, 2006; Abedin et al., 2006) respectively. Ahmed (2006) has the problem of low

*Corresponding author. E-mail: nzml_hasan@yahoo.com, Tel: +8801670931619.

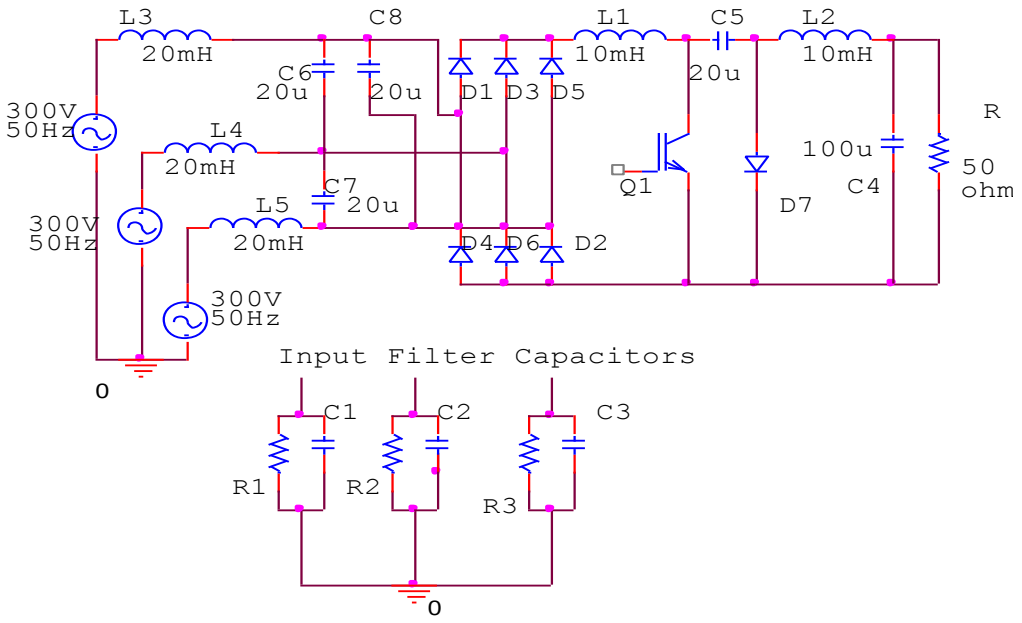

Figure 1. Circuit diagram of three phase Ĉuk rectifier with passive input filter and variable carrier frequency.

efficiency and Abedin et al. (2006) is not practically implementable due to large voltage drop across filters. The main objectives of this research work are (a) to propose a new control strategy to improve the performance of a Ĉuk regulator, (b) to simulate and study the new scheme under proposed control strategy for input current improvement of three phase diode rectifier, (c) total design of the input filter to reduce total harmonics distortion (THD) and hence reduce the input current of the converter, and (d) to increase the overall efficiency of the converter.

PROPOSED ĈUK REGULATOR

A Ĉuk regulator was investigated here to improve the overall performance to overcome the limitation of the fixed output voltage. A new strategy was introduced into the work. To avoid wide range of harmonics at the input current, the variable frequency control scheme was applied here by which the harmonics at the input current was limited within a certain range for all duty cycle (Figure 1). It is expected that the study will yield a three phase rectifier with improved power quality which is practically implementable for medium power application.

RESULTS AND DISCUSSION

The shape of the input current indicates that the performance of the regulator was improved. The simulated input current with 60% duty cycle is shown in Figure 8. Distortion free sinusoidal input current is a major consideration in a rectifier design. Many techniques have been developed by researchers in previous works. But large input filter and complex control strategy was the limitation for practically implementing of these regulators. Another important thing is, regulated output voltage both below and above the input voltages are required in many cases. Only Ĉuk and Buck-Boost regulators are able to supply regulated voltage below and above the input voltage. In this paper, a Ĉuk regulator is proposed for improvement of input current and efficiency of a three phase rectifier. At first a three phase full wave diode rectifier has been studied. The input current was found non sinusoidal pulsating and THD was found 25%. A passive filter was introduced to improve the performance of the rectifier. THD was improved to 2% and the efficiency was improved to 94%. But input for this performance 100uf input capacitor is required which is very large and also draw high input current. As a result, the VA rating of the rectifier increases and weight becomes large. The output voltage was not controllable.

To overcome the problems, a Ĉuk regulated three phase rectifier has been studied without input filter. It was observed that the input current was highly distorted with large THD, though the efficiency was good. The output voltage is controllable. To improve the shape of input current of Ĉuk regulated three phase rectifier with passive input filter was studied. The switching frequency was kept constant. It was found from the analysis that the THD has improved for many of the duty cycles, but the overall efficiency of the regulator was not acceptable at all duty cycles. It was also observed that efficiency and THD cannot be kept at the desired level simultaneously with change in duty cycle.

To improve the overall efficiency and to maintain the

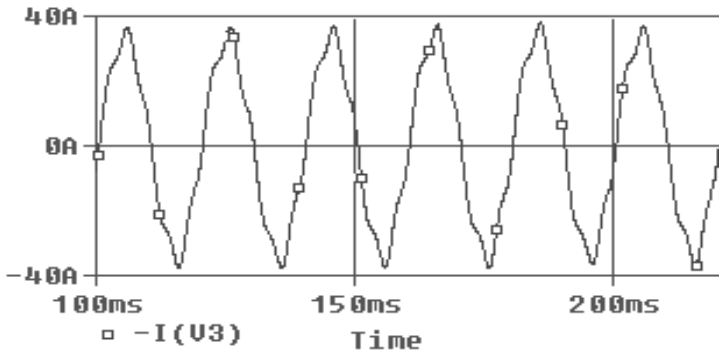

Figure 2. Input current of Ĉuk regulated three phase rectifier with passive input filter (duty cycle=60% and switching frequency= 2kz).

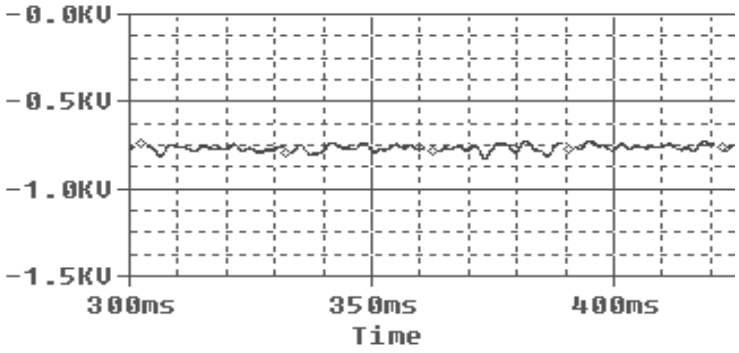

Figure 3. Output voltage of Ĉuk regulated three phase rectifier with passive input filter.

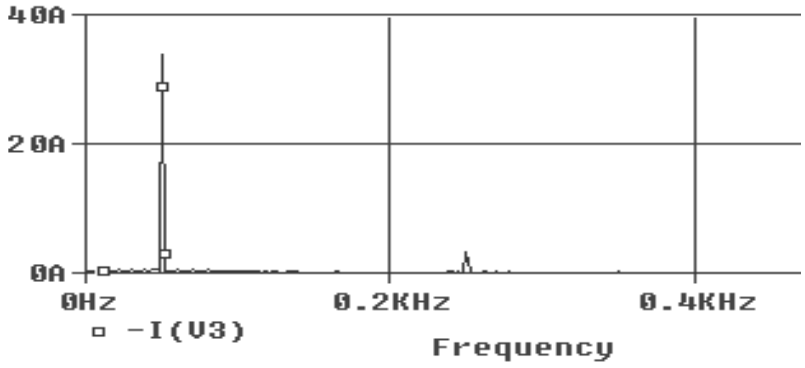

Figure 4. Typical FFT of input current of a Ĉuk regulated three phase rectifier.

THD of the input current at acceptable limit, a new topology was proposed and studied. A mixed passive filter was introduced at the input side of a Ĉuk regulator. At the same time, the switching frequency was varied from low to high frequency together with the variation duty cycles. It was found that highest THD was 7.533461% for 60% duty cycle which is below the tolerance level. The output voltage was varied from 187 volts to 770 volts with equal or more than 80% efficiency at all duty cycle. The value of input current was also acceptably low.

Input current, output voltage, FFT of input current, efficiency and power factor of the proposed Ĉuk regulator are shown in Figures 2 to 6 respectively. The overall performance of the proposed Ĉuk regulator can be understood in Table 1. The duty cycle versus power

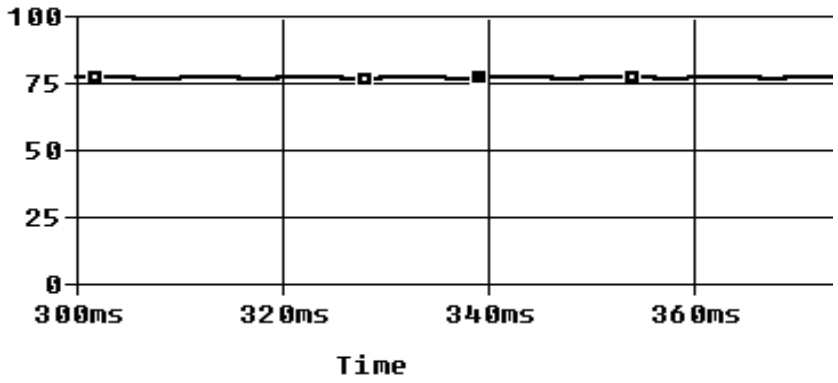

Figure 5. Efficiency of a Ĉuk regulated three phase rectifier.

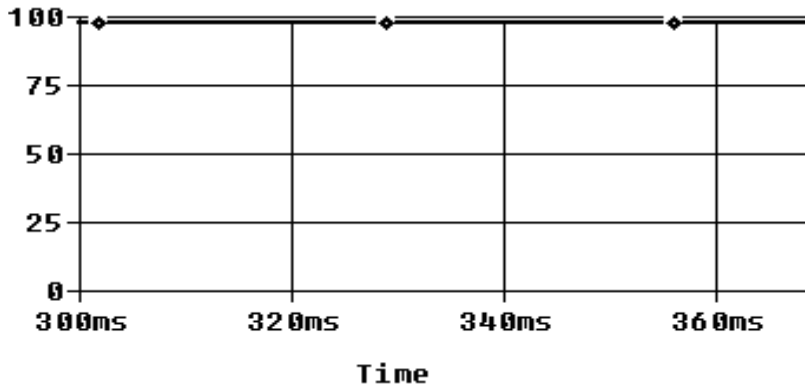

Figure 6. Power factor of Ĉuk regulated three phase rectifier with passive input filter.

Table 1. Performance parameter of Ĉuk regulator.

Duty cycle(%)	Frequency (KHz)	Input voltage (Volt)	THD (%)	PF (%)	Efficiency (η)%	Output voltage (Volt)
10	.75	300	3.144534E+00	21	82	187
20	1	300	5.868050E+00	47	94	310
30	1.25	300	5.265780E+00	65	99	400
40	1.5	300	5.247629E+00	76	92	460
50	1.75	300	7.149165E+00	91	91	600
60	2.00	300	7.533461E+00	98	80	770

factor, efficiency, output voltage, THD and switching frequency are shown in Figures 7 to 11.

Control strategy

A microcontroller based control system was introduced here. PWM modulation technique is applied to vary the duty cycle. Different duty cycles at different frequency have been generated by the microcontroller based circuit system. Practically generated pulse and flow chat of the program for generating pulse is given in Figures 12 and 13 respectively.

Conclusion

Three-phase PWM Ĉuk rectifiers have been investigated

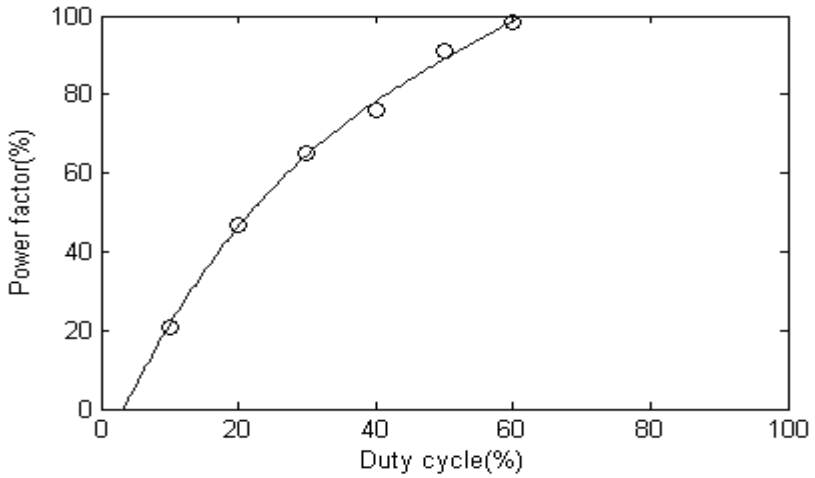

Figure 7. Duty cycle versus power factor.

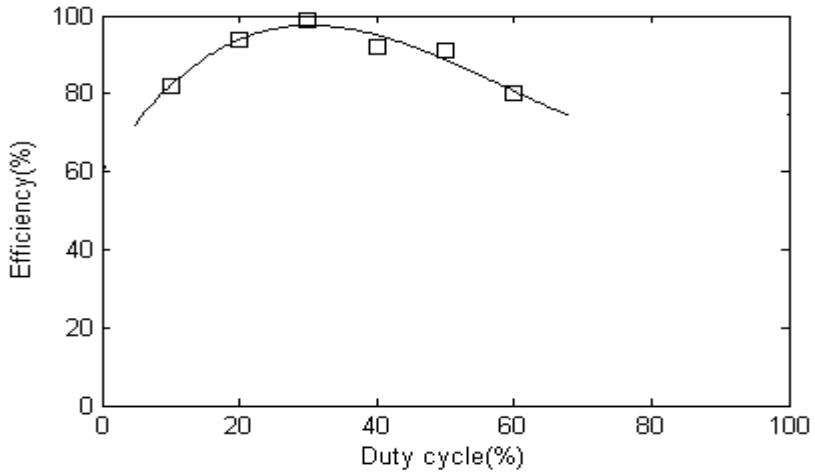

Figure 8. Duty cycle versus efficiency.

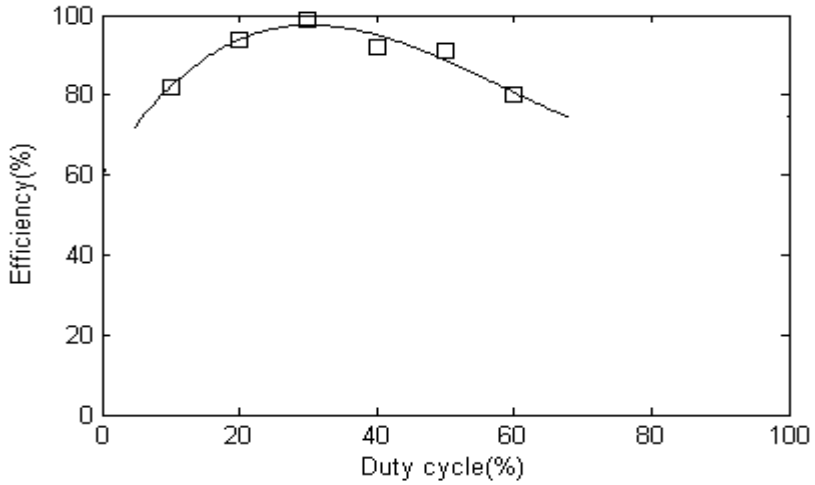

Figure 9. Duty cycle versus output voltage.

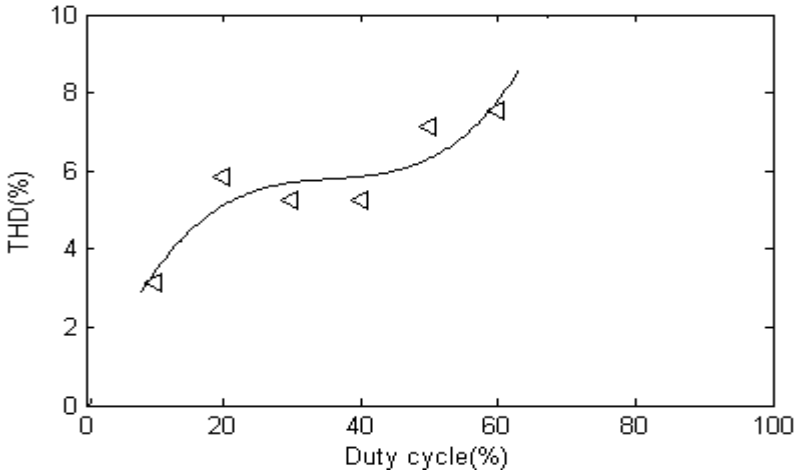

Figure 10. Duty cycle versus THD (%).

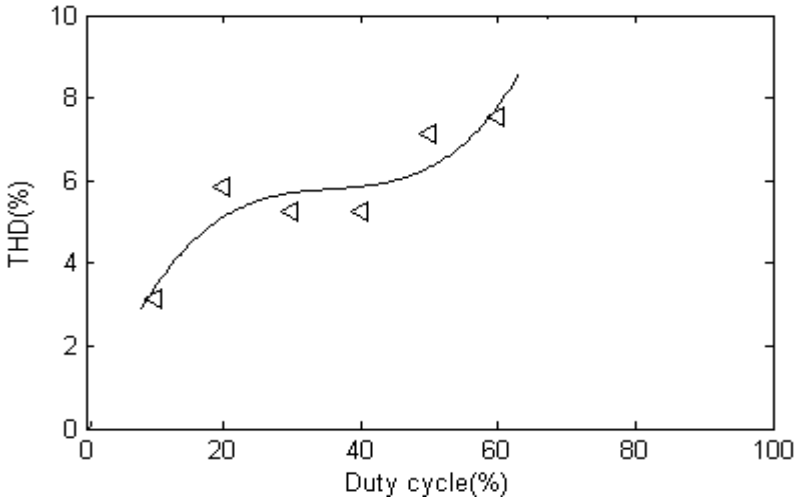

Figure 11. Duty cycle versus switching frequency.

Figure 12. Microcontroller generated pulse.

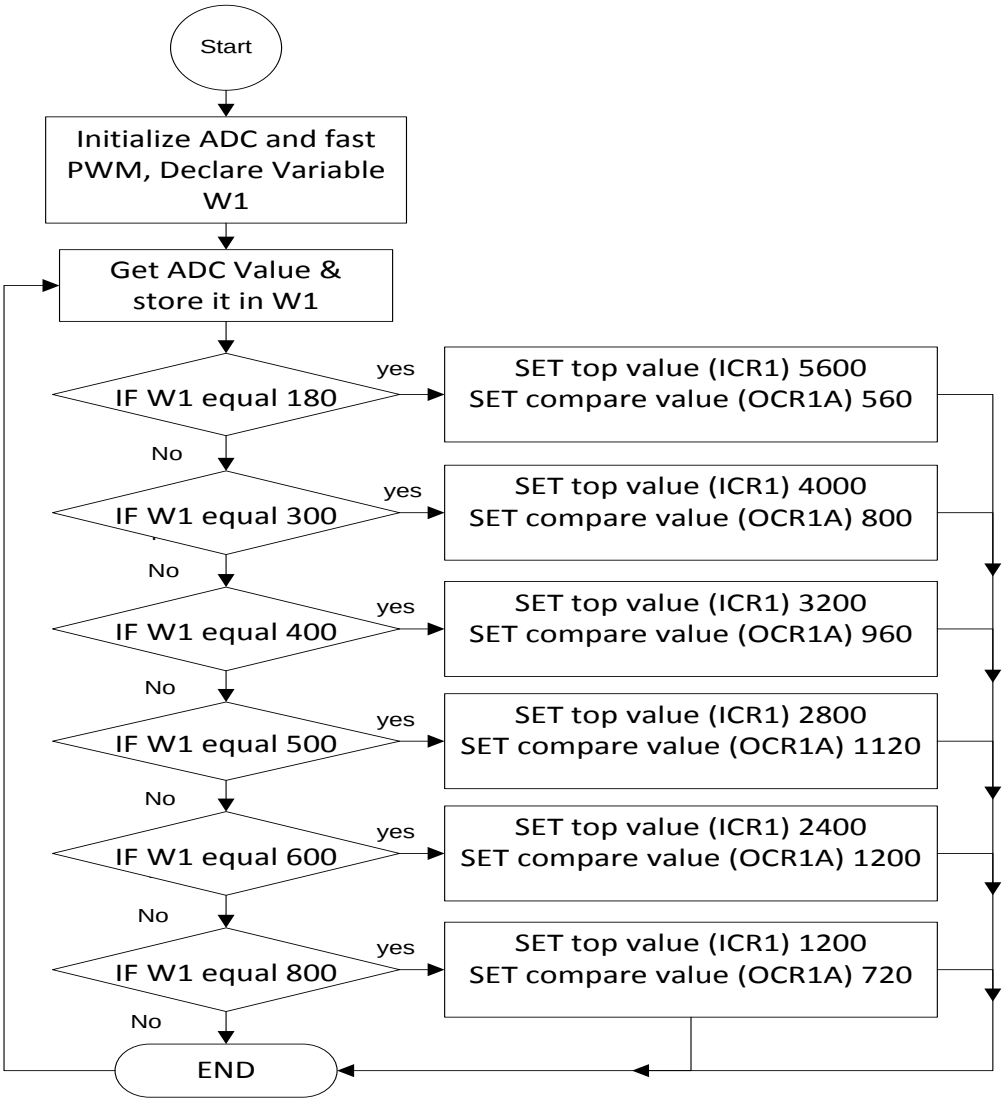

Figure 13. Flow chat of the program for generating pulse.

in this paper. The converters of interest have the properties of:

(1) Capabling both voltage step-up and step-down.
(2) Efficiency over 80% at all duty cycle.
(3) Almost sinusoidal input current. The simulated results have been presented here.

ACKNOWLEDGEMENTS

The authors acknowledge gratefully the support and facilities extended by the International Islamic University Chittagong (Dhaka Campus) and Department of Electrical and Electronic Engineering, Bangladesh University of Engineering and Technology, Dhaka, Bangladesh.

REFERENCES

Abedin AH, Ahmed MR, Alam MJ (2006). Improvement of input side current of three phase rectifier combining active and passive filters. J. Electric. Eng. IEB, EE 33(I- II):87-90, December 2006.
Ahmed MR (2006). Design of a switch mode ac Voltage regulator with improved power factor. M. Sc. Engineering Thesis, BUET, Department of EEE.
Alomgir H (2005). AC voltage regulation by Ĉuk switch mode power supply. M.Sc. Engineering Thesis, Department of EEE, BUET.
Blasko V, Kaura V (1997). A new mathematical model and control of athree-phase ac–dc voltage source converter. IEEE Trans. Power Electron. 12:116–123.
Busse A, Holtz J (1982). Multiloop control of a unity power factor switching ac to dc converter. Proc. IEEE PESC. 82:171–179.
Habetler TG (1993). A space vector-based rectifier regulator for ac/dc/ac converters. IEEE Trans. Power Electron. 8:30–36.
Kataoka T, Mizumachi K, Miyairi S (1979). A pulse width controlled ac-to-dc converter to improve power factor and waveform of ac line current. IEEE Trans. Ind. Appl. IA-15:670–675.
Kikuch L, Thomas LA (2002). Three-phase PWM Buck-Boost rectifiers with power regenerative capability. IEEE Trans. Ind. Appl. 1(5):

1361-1369.
Ooi BT, Salmon JC, Dixon JW, Kulkarni AB(1985). A 3-phase controlled current PWM converter with leading power factor. Int Conf. Rec. IEEE-IAS Annu. Meet. pp. 1008–1014.
Ruma B (2008). Input Current Improvement of a Three Phase Rectifier by Ĉuk regulator. M.S.c Engg thesis, Department of EEE, BUET, Dhaka, Bangladesh.
Wiechmann EP, Ziogas PD, Stefanovic VR (1984). A novel bilateral power conversion scheme for variable frequency static power supplies. Proc. IEEE PESC 84:388–396.
Wu R, Dewan SB, Slemon GR (1991). Analysis of an ac-to-dc voltage source converter using PWM with phase and amplitude control. IEEE Trans. Ind. Appl. 27:355–364.
Wu R, Dewan SB, Slemon GR(1988). A PWM ac to dc converter with fixed switching frequency, Int. Conf. Rec. IEEE-IAS Annu. Meet. pp. 706–711.
Ziogas PD, Kang YG, Stafanovic VR (1985). PWM control techniques for rectifier filter minimization. IEEE Trans. Ind. Appl. IA-21:1206–1214.

academicJournals

Vol. 8(35), pp. 1761-1771, 23 September, 2013
DOI: 10.5897/IJPS2013.3983
ISSN 1992 - 1950 © 2013 Academic Journals
http://www.academicjournals.org/IJPS

International Journal of Physical Sciences

Full Length Research Paper

Geoelectrical studies for the delineation of potential groundwater zones at Oduma in Enugu State, Southeastern Nigeria

Austin, C. OKONKWO and Isaac, I. UJAM

Department of Geology and Mining, Enugu State University of Science and Technology, Enugu, Nigeria.

Accepted 09 September, 2013

This work evaluates the use of geoelectrical method in the delineation of potential groundwater zones at Oduma in Enugu state, Southeastern Nigeria. Oduma lies within latitudes 6°02/ N to 6°07/ N and longitudes 7°35/ E to 7°41/ E with an area extent of about 102.6 km^2. The area is underlain by Awgu Shale group with its lateral arenaceous facie; Owelli Sandstone outcropping south of Oduma. Thirteen (13) vertical electrical soundings (VES) were carried out within the study area. Interpretated VES data shows predominance of Q and H curve type, indicating a fracture-shale subsurface. Contour maps of iso-resistivity, depth, transverse resistance, longitudinal conductance, aquifer transmissivity and hydraulic conductivity were constructed. Computed aquifer transmissivity from VES data values indicates a low yield aquifer. The latter was used to delineate the potential groundwater zones based on Gheorge aquifer transmissivity classifications. Comparisons of aquifer hydraulics estimated from geoelectrical sounding and the pump test analysis indicates a fairly good match. Three potential groundwater zones were delineated; the low, very low and negligible potential zones. The various contour maps and potential groundwater zone map will serve as a useful guide for groundwater exploration in the study area.

Key words: Resistivity, transmissivity, hydraulic conductivity, groundwater zones, aquifer yield.

INTRODUCTION

Oduma lies within latitude 6°02/ N to 6°07/ N and longitudes 7°35/ E to 7°41/ E with an area extent of about 102.6 km^2. It is located in Aninri local government area, Enugu state, southeastern Nigeria (Figure 1). The increasing population within Oduma and neigbouring towns has necessitated the high demand of groundwater development in the area. Cases of abortive water wells have been reported within Oduma and environs. Knowledge of groundwater zone is essential for a robust groundwater development program in the area. The natural flow of water through an aquifer is determined from the hydraulic properties of the aquifer. Hydraulic conductivity (k), transmissivity (T) and storativity (S) are the aquifer properties. Transmissivity is the hydraulic conductivity multiplied by the saturated thickness of the aquifer. Predictions of these hydraulic properties are mainly from pumping test analysis. Now geophysical methods provide an effective technique for aquifer evaluation. Estimates of hydraulic properties from geoelectrical soundings have been made by several authors (Ezeh and Ugwu, 2010; Kelly, 1979; Urish, 1987). These parameters were estimated using empirical and semi-empirical relationships (Huntly, 1987; Koinski, 1981). Their study was aimed at characterizing the aquifers for optimum yield.

In the present study, an attempt has been made by

*Corresponding author. E-mail: okonkwo.austin@esut.edu.ng

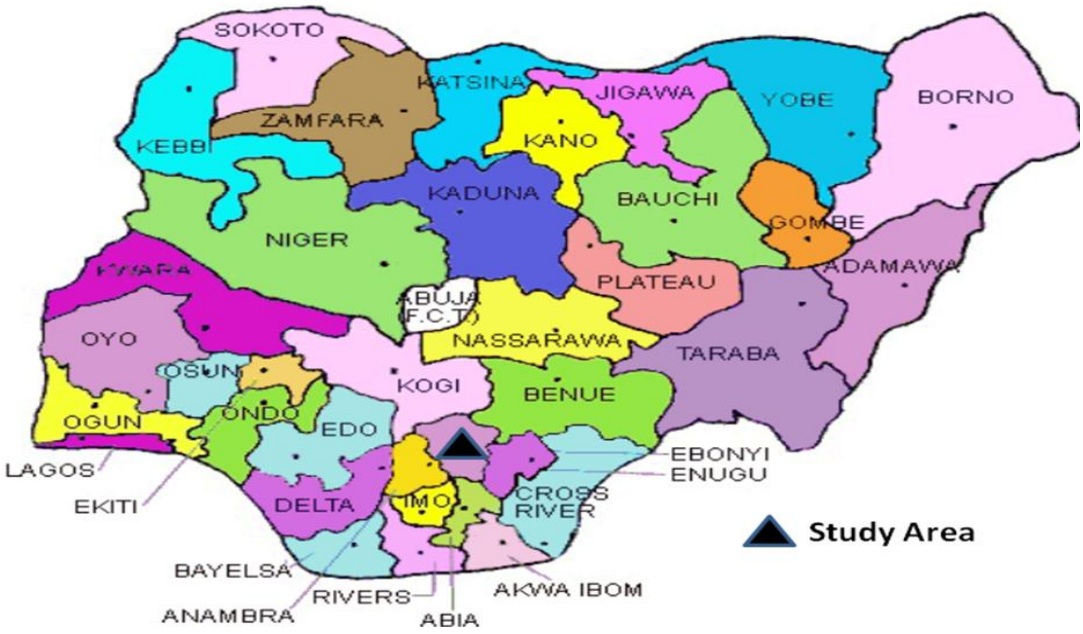

Figure 1. Map of Nigeria showing the study area (World Gazette, 2011).

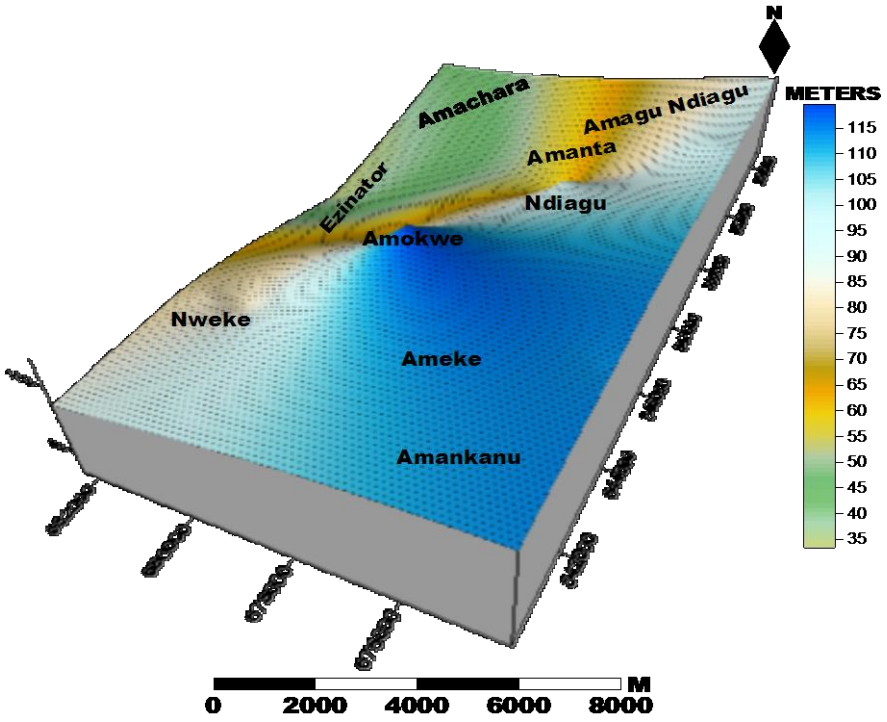

Figure 2. Surface map of the study area.

using the distribution of these hydraulic parameters to delineate the groundwater potential zone at Oduma and environs. Modeled estimates of the hydraulic parameters from geoelectrics were compared with data from pumping test to have a better picture of groundwater potential zone.

Study area

Physiography

The study area is fairly a lowland topography (Figure 2). Amokwe community is about the highest in the area, with

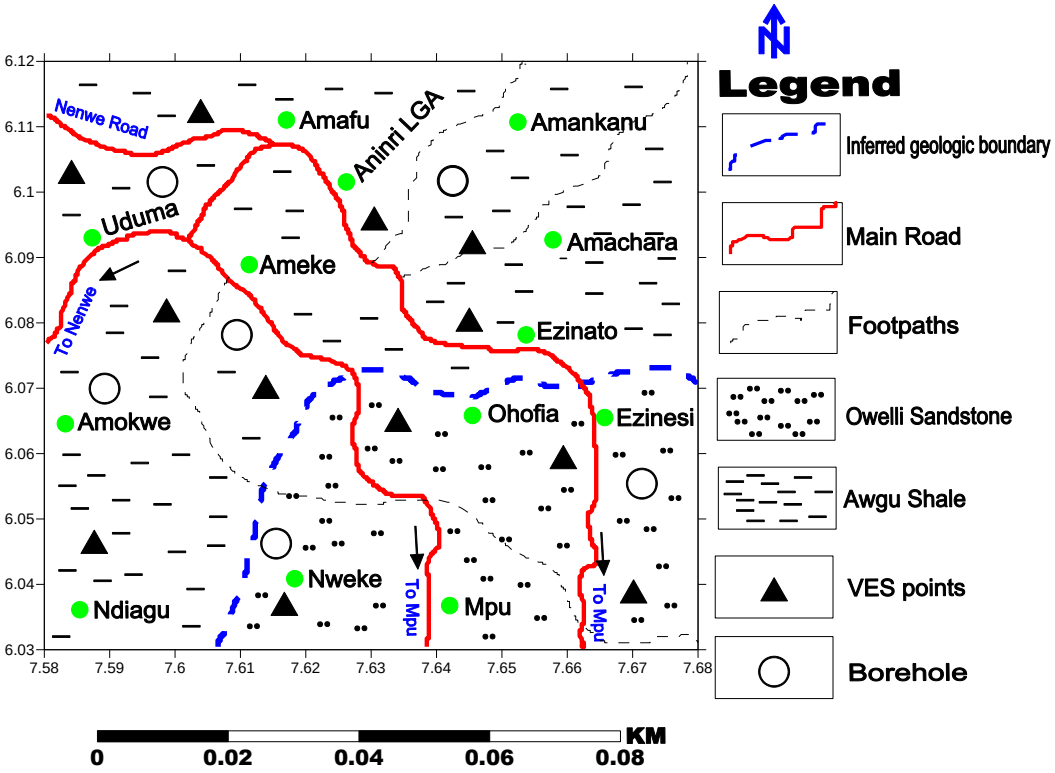

Figure 3. Geologic map of the study area showing VES stations and borehole points.

an elevation of 120 m above sea level (ASL). The lowland is indicative of the cultural land use system in the area. As the area is predominately rice farm terrain as a result of stagnant water, the flat topography is also controlled by the subsurface geology of the area.

Geology

The study area falls within the geologic complex called, the Lower Benue Trough. It is underlain by Awgu Shale unit which is coniacian in age, with an arenaceous facies (Owelli Sandstone) development to the south of Oduma (Figure 3). The unit consists of bluish grey, well bedded shales with occasional intercalations of fine-grained, pale yellow, calcareous sandstones and shaly limestones (Reyment, 1965). It is about 900 m thick and gently folded.

Hydrogeology

The study area falls within the Cross River Basin, which is hydrogeologically a problematic groundwater basin (Offordile, 2002). This is as a result of poor yield and saliferous groundwater. More than 90% of the basin is underlain by cretaceous rocks of the Asu River, Ezeaku, Awgu, Nkporo and Mamu Formations, with the oldest, the Asu River Formation, underlain by the basement complex rocks. With the exception of Awgu and Ezeaku formation, all these rock units are very poor aquifers. The sandstones within the Awgu formation are thin and generally limited in extent and as a result, give poor yields. Aneke (2007) proposed an exploration strategy for exploiting the groundwater from the fractured shaley units which are the main water bearing units in the study area.

THEORY AND METHODS

The electrical resistivity method is utilized in diverse ways for groundwater exploration (Zohdy, 1976; Choudhury et al, 2001; Frohlich and Urish, 2002). Electrical surveys are usually designed to measure the electrical resistivity of subsurface materials by making measurements at the earth surface. Current is introduced into the ground by a pair of electrodes, while measuring the subsurface expression of the resulting potential field with an additional pair of electrodes at appropriate spacing.

Data acquisition and interpretation

A total of thirteen vertical electrical sounding (VES) was acquired within and outside the study area (Figure 2). Some were stationed very close to existing boreholes, for correlation purposes. The Schlumberger electrode configuration was used with maximum current electrode separation ranging from 400 to 600 m. The equipment used for the fieldwork was the versatile Ohmega resistivity meter.

Table 1. Interpreted model geoelectric parameters and curve types from the study area.

S/N	Location	VES No	NL	ρ_1	ρ_2	ρ_3	ρ_4	ρ_5	ρ_6	ρ_7	ρ_8	T_1	T_2	T_3	T_4	T_5	T_6	T_7	Curve type
1	Nkwo Amorji	1	7	5	2	2	6	10	10	38	-	0.6	1.2	1.2	2.0	7.0	42.0	-	HA
2	Nawu Ezinesi	2	7	50	35	15	6	5	8	125	-	0.8	0.4	1.8	12.0	15.0	28.0	-	QQA
3	Ezinator	3	7	15	5	3	5	8	15	80	-	0.8	1.4	2.8	18.0	17.0	18.0	-	QAA
4	Nweke	4	7	380	220	100	20	5	105	1152	-	0.8	1.2	2.5	10.5	25.0	20.0	-	QQA
5	Ameke	5	7	1205	2785	12	14	23	4	35	-	0.8	1.1	2.6	20.5	31.0	69.0	-	KAH
6	Amaorji	6	7	280	225	18	9	7	6	18	-	0.8	1.7	2.0	5.5	32.0	93	-	QQH
7	Amankanu	7	7	750	520	40	18	4	2	85	-	1.0	1.5	5.0	14.5	43.0	63.0	-	QQH
8	Enugu Agu	8	7	780	120	18	25	24	11	55	-	0.8	1.7	4.3	18.2	31.0	64.0	-	QKH
9	Ndiagu	9	7	1002	3452	275	13	23	90	20	-	0.8	1.2	5.5	18.5	30.0	69.0	-	KHK
10	Amokwe	10	6	165	12	6	10	2	11	-	-	0.8	1.7	2.5	40.0	19.0	-	-	QK
11	Amanta	11	6	46	13	8	14	21	8	-	-	0.8	1.2	4.0	14.0	40.0	-	-	QA
12	Amachara	12	7	14	9	13	10	14	20	8	-	0.8	1.7	1.5	11.0	25.0	45.0	-	HHK
13	Amagu Ndiagu	13	5	105	75	22	2	250	-	-	-	0.8	1.4	7.8	15.0	-	-	-	QH

After acquiring the data, the measured field resistance (R) in ohms was converted to apparent resistivity (ρ_a) in ohm-meter by multiplying resistance (R) by the geometric factor (K). A log-log graph plot of apparent resistivity (ρ_a) against current electrode distance (AB/2) was plotted for each VES station to generate a sounding curve. Using the conventional partial curve matching technique, in conjunction with auxiliary point diagrams (Orellana and Mooney, 1966; Koefoed, 1979; Kellar and Frischknecht, 1966), layer resistivities and thickness were obtained, which served as a starting point for computer-assisted interpretation. The computer program RESOUND was used to interpret all the data sets obtained. From the interpretation of the resistivity data, it has been possible to compute for every VES station, the longitudinal conductance(S).

$$S = h_i/\rho_i \quad (1)$$

And transverse resistance(R)

$$R = h_i.\rho_i \quad (2)$$

Where h_i and ρ_i are thickness and resistivity of the aquiferous layer. These parameters R and S are known as the Dar-zarrouk variable and Dar-zarrouk function, respectively (Maillet, 1947). Further quantitative analysis for aquifer hydraulics in the study area are based on Equations 1 and 2 using analytical relationship of Niwas and Singhal (1981). They showed that: in areas of similar geologic setting and water quality, the product kσ (hydraulic conductivity) remain fairly constant.

Interpretation

The form of curves obtained by sounding over a horizontally stratified medium is a function of the resistivities and thicknesses of the layers as well as the electrode configuration (Zohdy, 1976). The resistivity curve type associated with the study area from VES 1-13 include: HA, QQA, QAA, QQA, KAH, QQH, QKH, KHK, QK, QA, HHK, and QH curve types respectively (Table 1). The first dominant curve type is Q. This is indicating a shaly terrain. The H curve type is the second dominant. This also indicates fractured shale horizons which are targets for groundwater exploration.

RESULTS AND DISCUSSION

Geoelectrical sounding

Contour maps of the apparent resistivity, the isopach, the depth, the longitudinal conductance, the transverse resistance, the transmissivity and the hydraulic conductivity of the aquiferous horizon have been constructed using the results of the resistivity sounding interpretation. Apparent resistivity variation (Figure 4) indicates a high resistivity to the southeast and southwest with low resistivity to the north, around Amokwe and Nawu Ezinesi. Aquifer depth variation is a function of topography. A NW-SE trend variation predominates (Figure 5). The isopach map also show similar trend (Figure 6). The distribution of the aquifer transverse resistance and longitudinal conductance computed from the VES interpretation is shown in Figures 7 and 8 respectively. Maximum values of transverse resistance are observed around Ndiagu-Nweke-Amachara axis. Aquifer transmissivity (Figure 9) does not show similar trend, with highest value of $11m^2$/day at Amachara, indicating a low permeability aquifer (Ekwe et al, 2010) and very low potential (Ezeh, 2012). The longitudinal conductance shows a thick resistive horizon at Amankanu and also in a NW-SE trend. Hydraulic conductivity computed from VES interpretation (Figure 10) show an aquifer with a poor yield, practically depicting a shaly terrain (Figure 12).

Borehole data

Aquifer parameters from pumping test analysis were also acquired. They are transmissivity (Figure 13), hydraulic conductivity (Figure 14) and aquifer yield (Figure 15). Contour maps for the former were also produced.

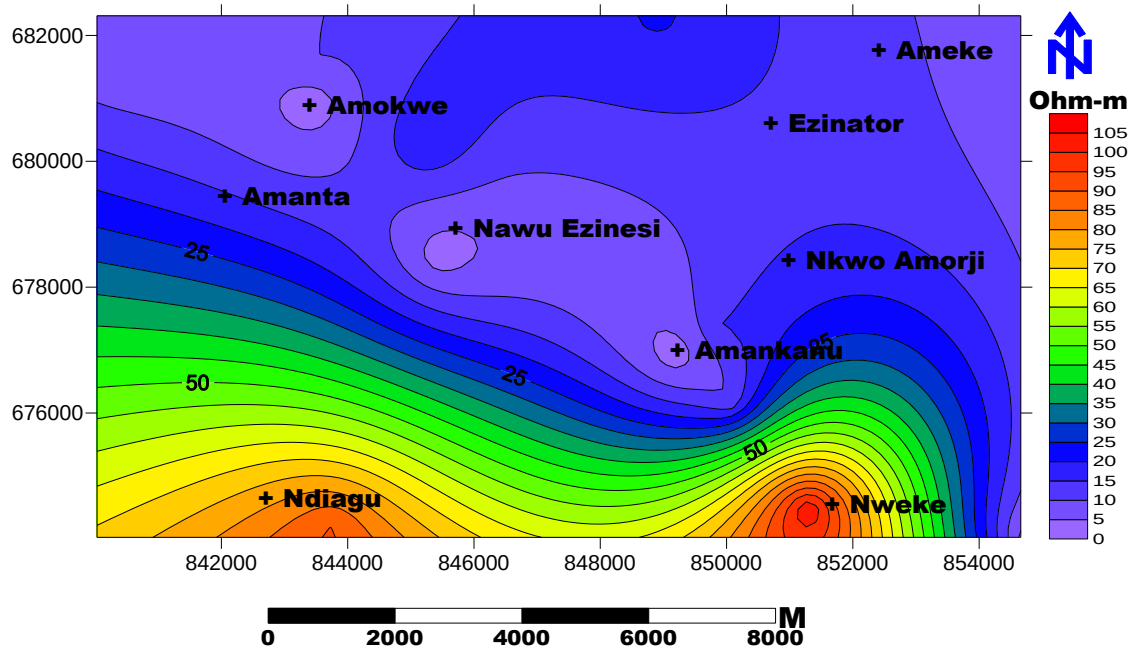

Figure 4. Iso-apparent resistivity map of aquiferous horizon in the study area.

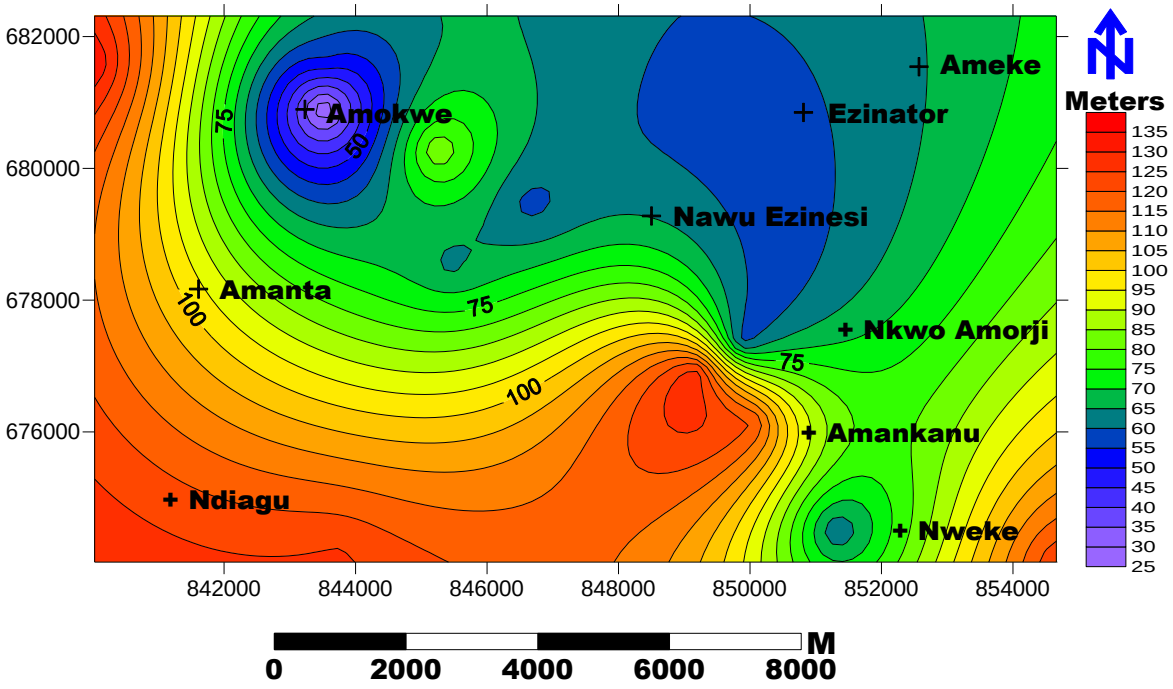

Figure 5. Aquifer depth map of the study area.

Comparisons of aquifer hydraulics estimated from geoelectrical sounding and the pump test analysis indicates a fairly good match. Estimated aquifer transmissivity (Figure 9) around Nweke, Amokwe, Amachara and Ndiagu fairly matches aquifer transmissivity from pump test data. Similarly the estimated hydraulic conductivity from geoelectrical sounding also fairly matches hydraulic conductivity from pumping test data in the study area. The aquifer yield (Figure 15) depicts the true picture of the study area as a

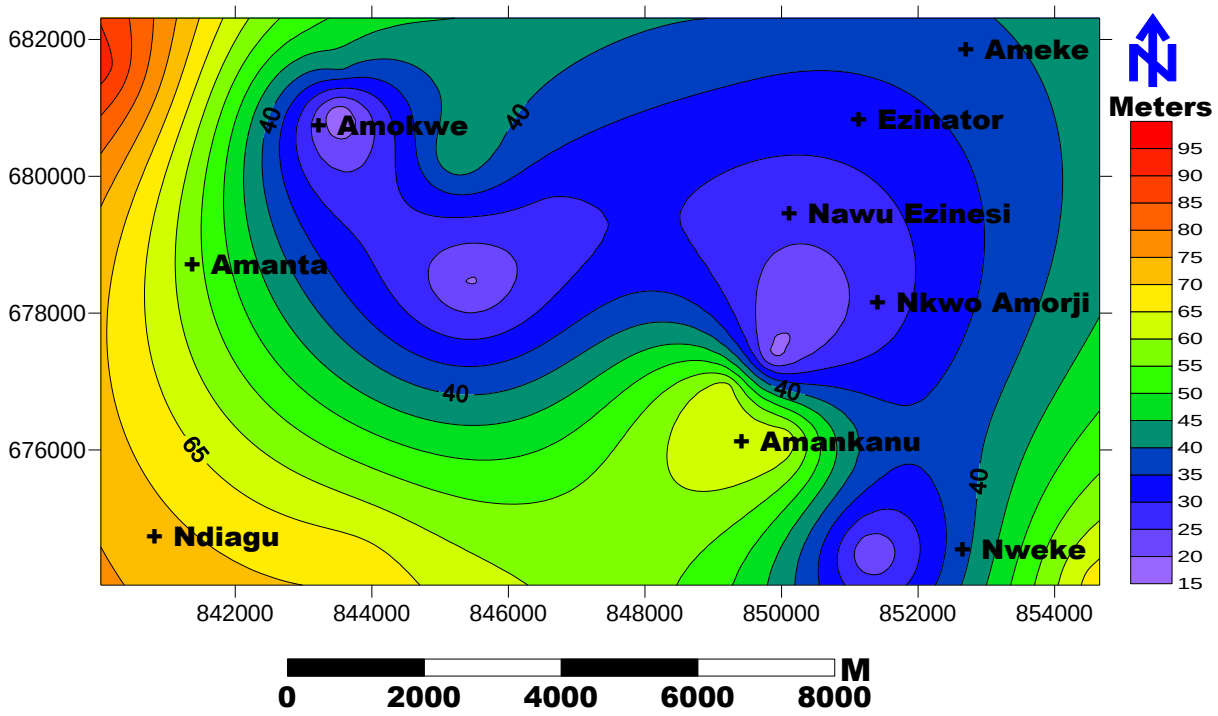

Figure 6. Isopach map of the aquiferous horizon in the study area.

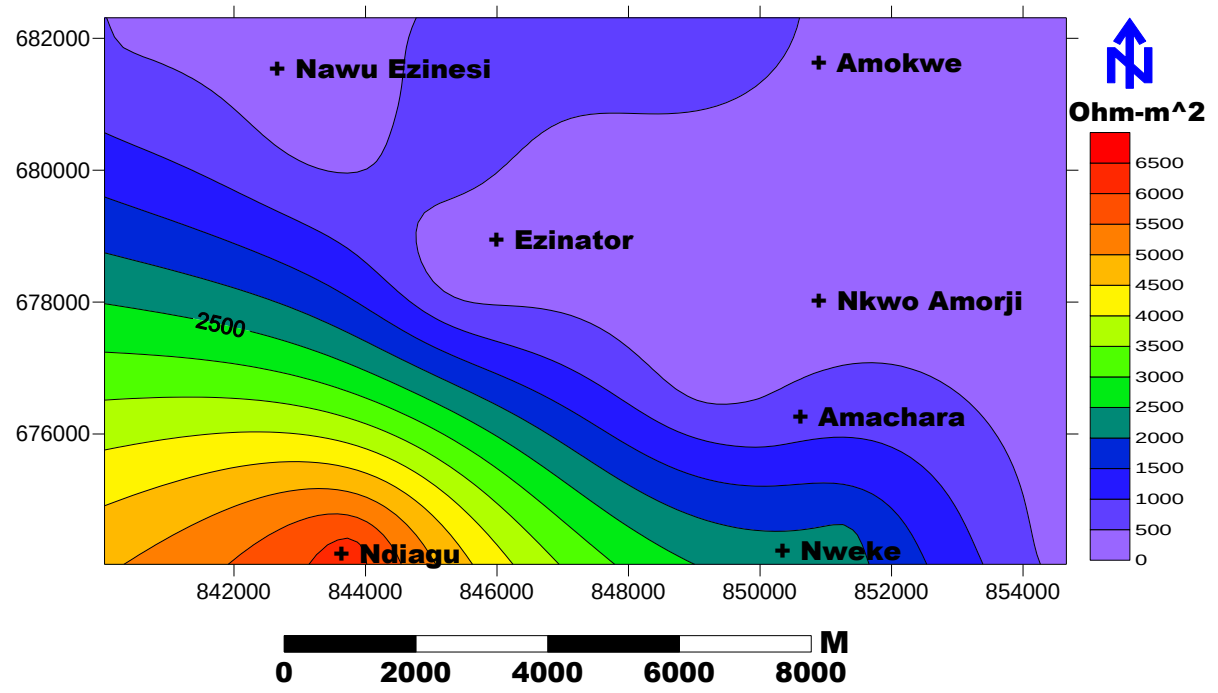

Figure 7. Transverse resistance map of the study area.

low permeability area. The highest aquifer yield in the area is about 6.20 m^3/h at southeast corner near Nweke village.

Groundwater potential evaluation

The groundwater potential zones was delineated (Figure

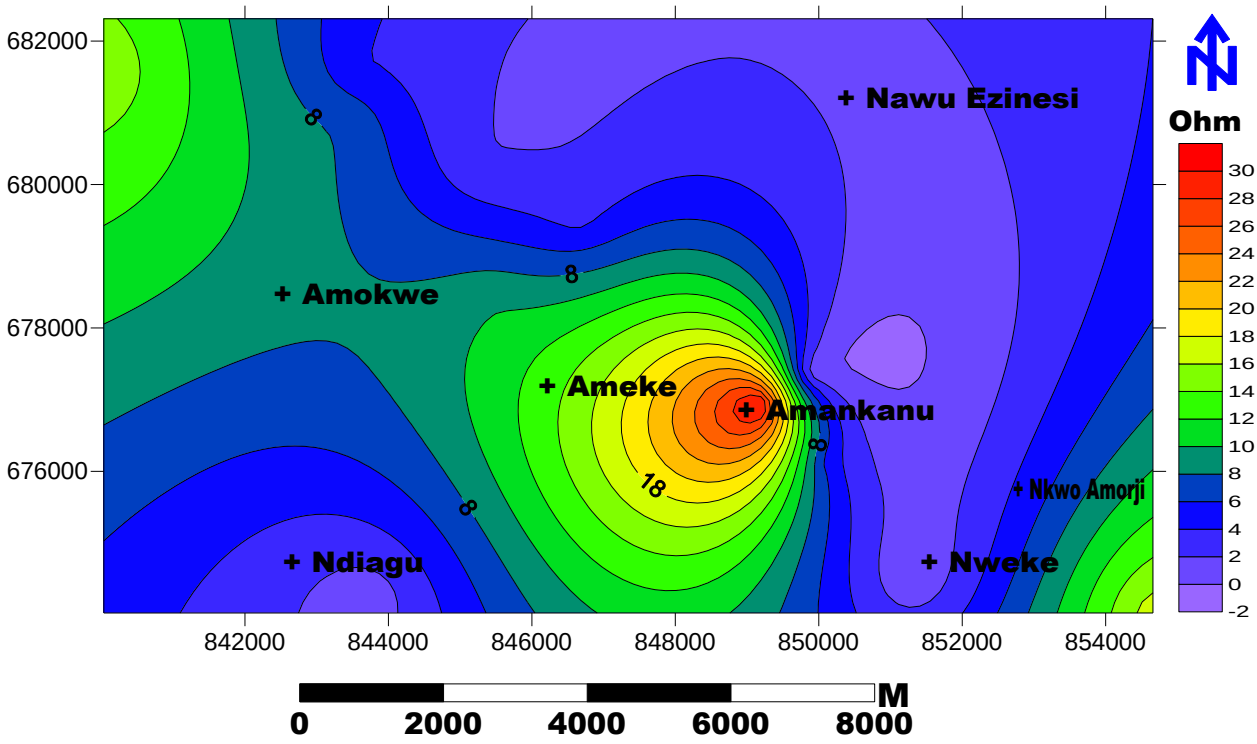

Figure 8. Longitudinal conductance map of the study area.

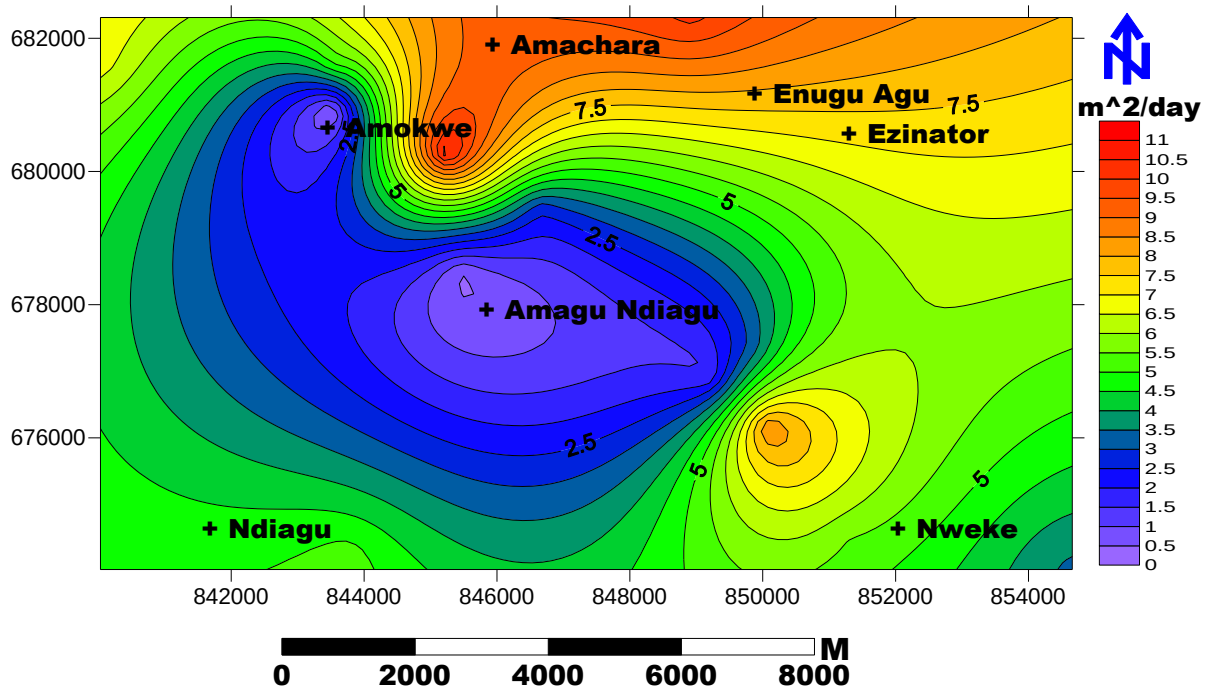

Figure 9. Aquifer transmissivity map of the study area.

11) based on Gheorghe (1978) aquifer transmissivity classifications. Groundwater potential is a function of complex inter-relationship between geology, physiography, groundwater flow pattern, recharge and

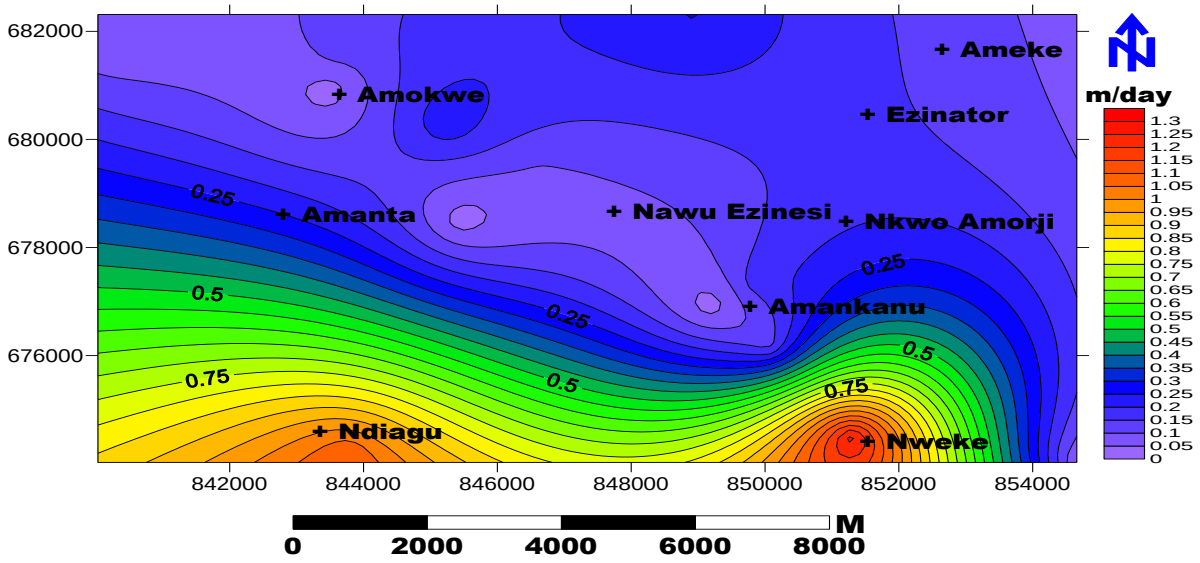

Figure 10. Aquifer hydraulic conductivity map of the study area.

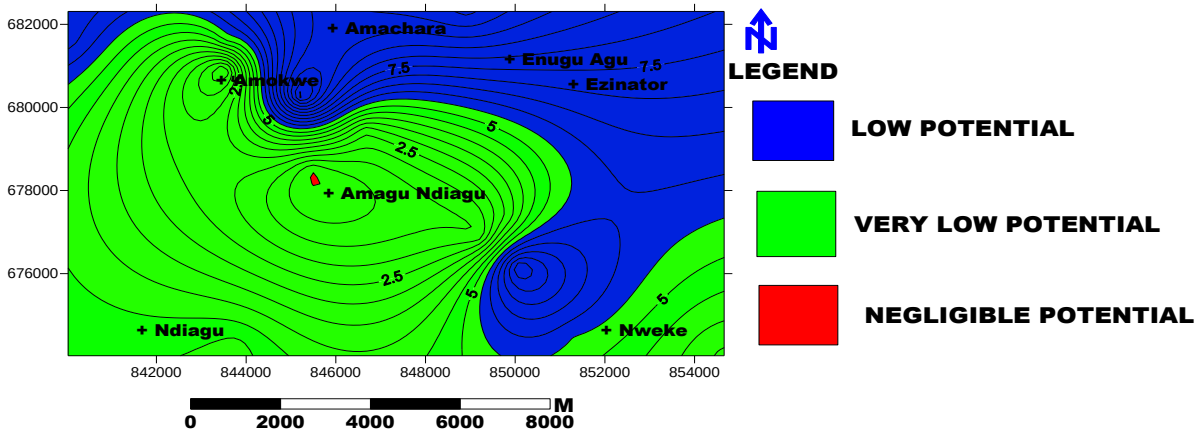

Figure 11. Groundwater potential zones of the study area.

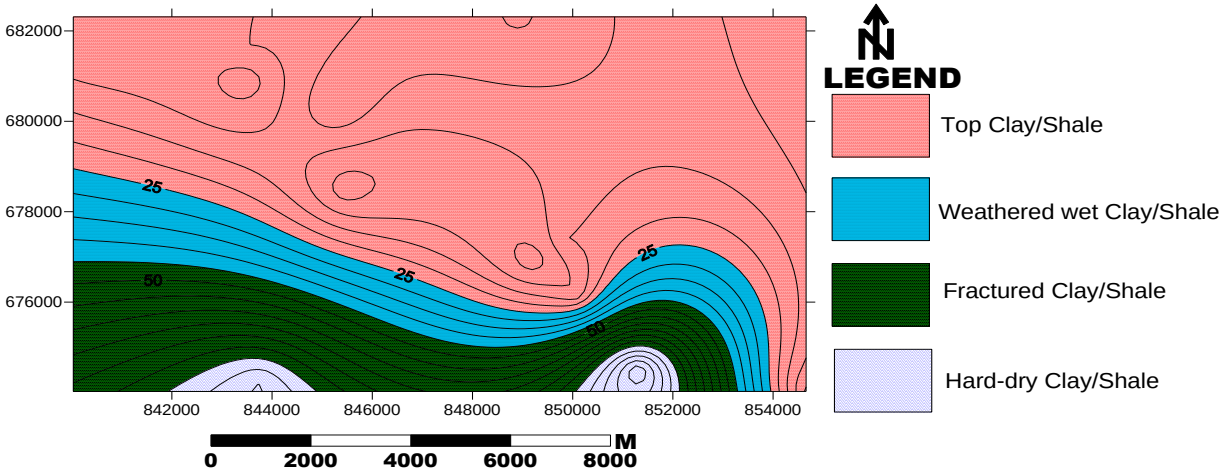

Figure 12. Possible geoelectric layer distribution.

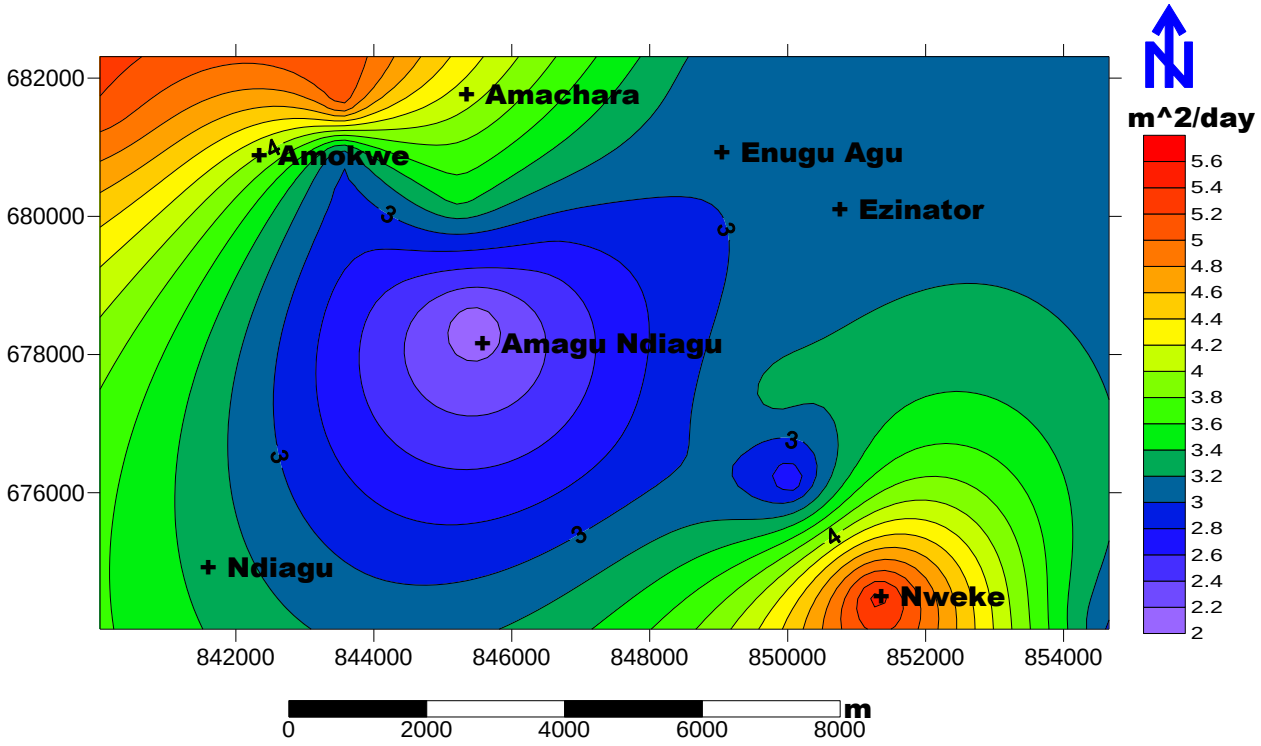

Figure 13. Aquifer transmissivity map (from pumping test analysis) of the study area.

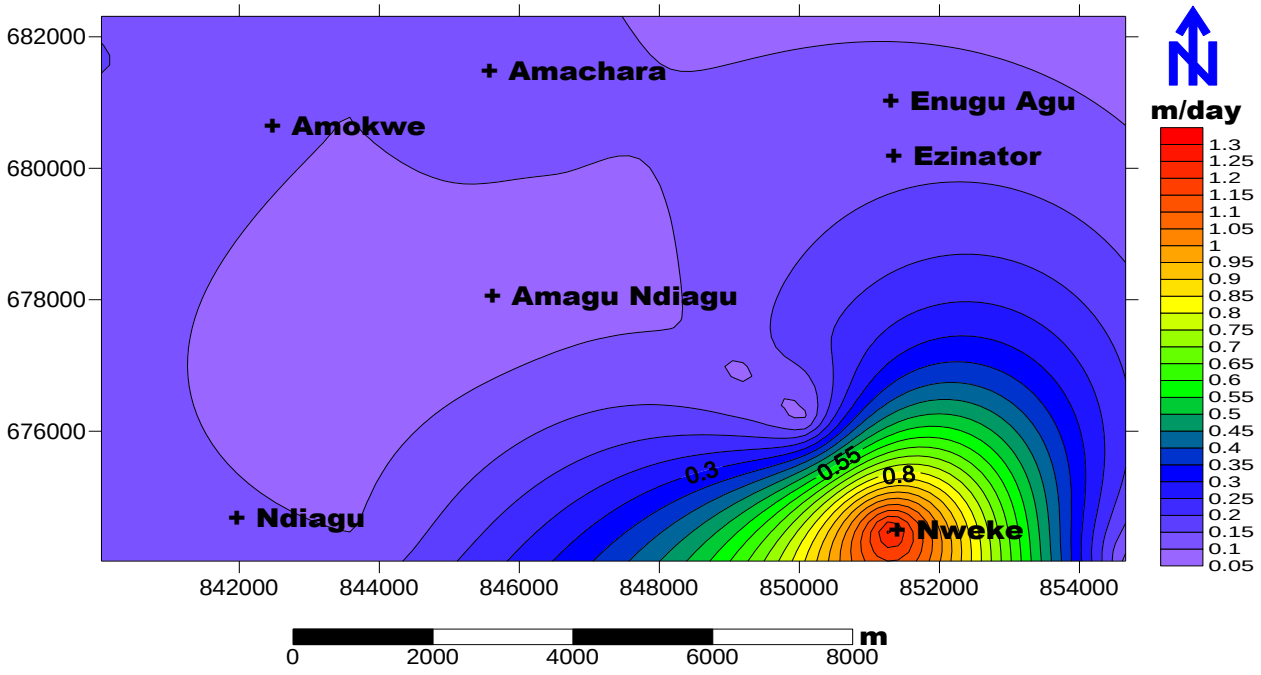

Figure 14. Aquifer hydraulic conductivity map (from pumping test analysis) of the study area.

discharge processes (Ezeh, 2012). The present evaluation of the groundwater potential of the study area has been based on aquifer geoelectrical parameters obtained from VES interpretation results. Three potential

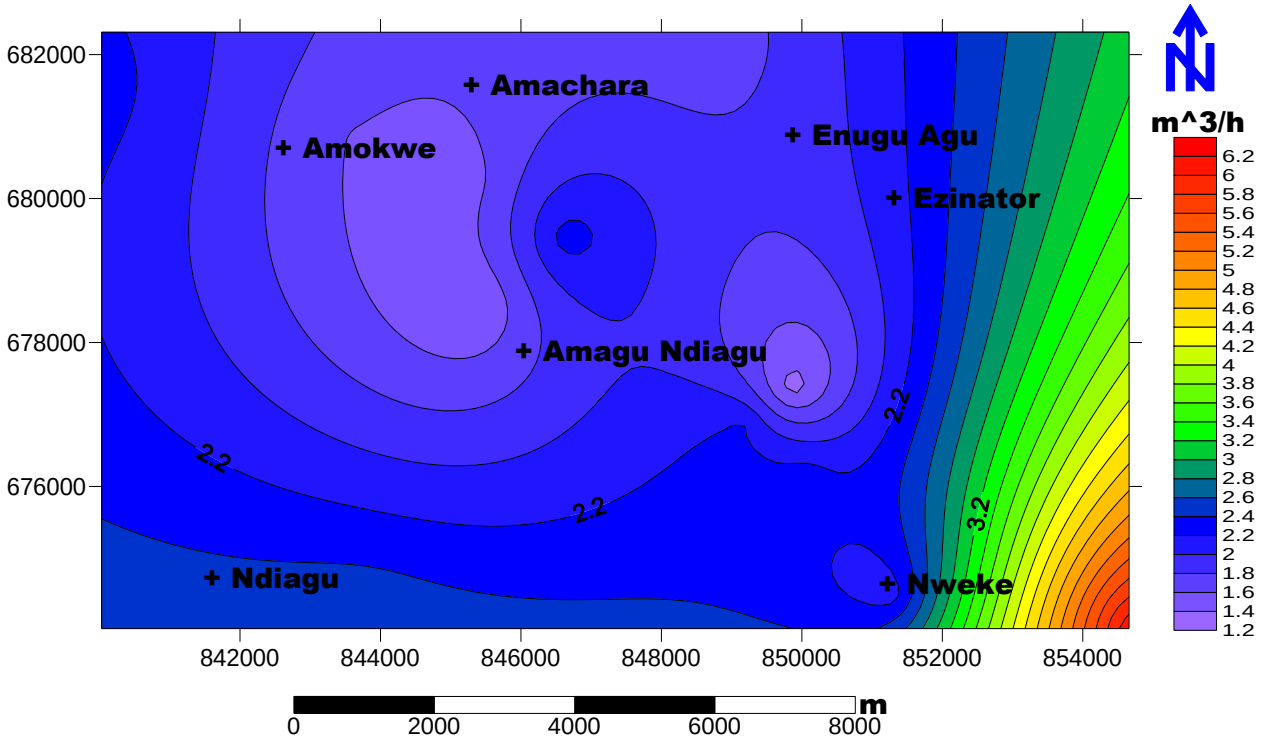

Figure 15. Aquifer yield map (from pumping test analysis) contour map from the study area.

groundwater zones were delineated. The zones are low, very low and negligible potentials. The country around Amagu Ndiagu, Ndiagu, Nweke and Amokwe are of very low potential while areas to the northeast around Enugu Agu, Ezinator and Amachara are of low potential. Negligible potential was quite insignificant.

Conclusion

Based on the geoelectrical studies, the potential groundwater zones were delineated; the low, very low and negligible potential zones. Computed aquifer hydraulics parameters indicate a low aquifer yield. However, this should not stall further groundwater exploration in the area but more detailed hydrogeological and geophysical investigations must be carried out to determine good point(s) for groundwater development. A depth greater than 60 m but less than 100 m may be recommended.

ACKNOWLEDGEMENT

The authors are grateful to EssBee Geotechnical ventures limited for the resistivity data processing. Many thanks to Mr. Emmanuel Enang, principal geologist Felgralinks Nigeria limited, for his qualitative role during the data acquisition stage.

REFERENCES

Aneke BC (2007). Water resources of the Awgu Shale group, Enugu state, southeastern Nigeria. Ph.D Thesis, University of Nigeria, Nsukka.

Choudhury K, Saha DK, Chakraborky P (2001). Geophysical study for saline water intrusion in a coastal alluvial terrain. J. Appl. Geophys. 46:189-200.

Ekwe AC, Nnodu IN, Ugwumbah KI, Onwuka OS (2010). Estimation of aquifer hydraulic Characteristics of low permeability formation from geosounding data: A case study of Oduma Town, Enugu State. J. Earth Sci. 4(1):19-26.

Ezeh CC (2012). Hydrogeophysical studies for the Delineation of potential groundwater zones In Enugu State, Nigeria. Int. Res. J. Geol. Min. 2(5):103-112.

Ezeh CC, Ugwu GZ (2010). Geolectrical sounding for estimating groundwater potential in Nsukka L.G.A. Enugu State, Nigeria. Int. J. Phys. Sci. 5(5):415-420.

Frohlich RK, Urish D (2002). The use of geoelectrics and test wells for the assessment of Groundwater quality of a coastal industrial site. J. Appl. Geophys. 46:261-278.

Gheorge A (1978). Processing and synthesis of hydrogeological data. Abacus press, Tunbridge, Kent. 136 pp.

Huntly D (1987). Relations between permeability and electrical resistivity in granular aquifers. Groundwater 24:466-474.

Kelly WE (1979). Geoelectric sounding for estimating aquifer hydraulic conductivity. Groundwater 50(6):420–425.

Keller GV, Frischknecht FC (1966). Electrical methods in geophysical prospecting. Pergamon Press.

Koefoed O (1979). Geosounding principles, 1 Elsevier, Amsterdam.

Koinski WK (1981). Geolectric soundings for predicting aquifer properties. Groundwater 19(2):163-171.

Maillet R (1947). The fundamental equations of electrical prospecting. Geophysics 12:529-556.

Niwas S, Singhal DC (1981). Estimation of aquifer transmissivity from Dar-zarrouk parameters in porous media. J. Hydrol. 50:393-399.

Offordile ME (2002). Groundwater study and development in Nigeria. 2nd Edition. Mecon geology And Engineering Services Ltd. Jos, Nigeria. 453 pp.
Orellana E, Mooney HM (1966). Master tables and curves for vertical electrical sounding over Layered structures. Interscience, Madrid.
Urish DW (1987). Electrical resistivity-hydraulic conductivity relationships in glacial outwash aquifers. Water Resour. Res. 17(5):1401-1408.
World Gazette (2011). Colourful map of Nigeria with 36 states. www.world-gazette.com
Zohdy AAR (1976). Application of surface geophysical (electrical methods to groundwater Investigations) techniques of water resources investigations of the United States Geological Survey pp. 5-55.

14th International Conference on Accelerator and Large Experimental Physics Control Systems. The Hyatt Regency Embarcadero Center San Francisco, California October 6-11, 2013

December 6-7, 2013 Sydney, Australia 2013 5th International Conference on Signal Processing Systems

Conferences and Advert

October 2013
14th International Conference on Accelerator and Large Experimental Physics Control Systems. The Hyatt Regency Embarcadero Center San Francisco, California October 6-11, 2013

December 2013
5th International Conference on Signal Processing Systems Sydney, Australlia, December 6-7, 2013

International Journal of Physical Sciences

Related Journals Published by Academic Journals

- *African Journal of Pure and Applied Chemistry*
- *Journal of Internet and Information Systems*
- *Journal of Geology and Mining Research*
- *Journal of Oceanography and Marine Science*
- *Journal of Environmental Chemistry and Ecotoxicology*
- *Journal of Petroleum Technology and Alternative Fuels*

academicJournals